Clathrin-mediated Endocytosis Facilitates Internalization of *Magnaporthe oryzae* Effectors into Rice Cells

Ely Oliveira-Garcia[1,2]*, Tej Man Tamang[1,3], Jungeun Park[3], Melinda Dalby[1], Magdalena Martin-Urdiroz[4], Clara Rodriguez Herrero[4,5], An Hong Vu[2], Sunghun Park[3], Nicholas J. Talbot[5] & Barbara Valent[1]*

[1]Department of Plant Pathology, Kansas State University, Manhattan, KS 66506, U.S.A.
[2]Department of Plant Pathology and Crop Physiology, Louisiana State University Agricultural Center, Baton Rouge, LA 70803, U.S.A.
[3]Department of Horticulture and Natural Resources, Kansas State University, Manhattan, KS 66506, U.S.A.
[4]School of Biosciences, University of Exeter, Exeter, EX4 4QD, UK
[5]The Sainsbury Laboratory, University of East Anglia, Norwich Research Park, Norwich NR4 7UH, UK.

*Corresponding authors: E. Oliveira-Garcia; E-mail: EOliveiraGarcia@agcenter.lsu.edu and B. Valent; E-mail: bvalent@ksu.edu

Short Title: Blast Effector Translocation By Plant Endocytosis

* The author(s) responsible for distribution of materials integral to the findings presented in this article in accordance with the policy described in the Instructions for Authors (https://academic.oup.com/plcell/pages/General-Instructions) are: E. Oliveira-Garcia (EOliveiraGarcia@agcenter.lsu.edu) and B. Valent (bvalent@ksu.edu).

ABSTRACT

Fungi and oomycetes deliver effectors into living plant cells to suppress defenses and control plant processes needed for infection. Little is known about the mechanism by which these pathogens translocate effector proteins across the plasma membrane into the plant cytoplasm. The blast fungus *Magnaporthe oryzae* secretes cytoplasmic effectors into a specialized biotrophic interfacial complex (BIC) before translocation. Here we show that cytoplasmic effectors within BICs are packaged into vesicles that are occasionally observed in the host cytoplasm. Live cell imaging with fluorescently-labeled rice showed that effector vesicles colocalize with plant plasma membrane and with clathrin light chain-1, a marker for clathrin-mediated endocytosis (CME). Inhibition of CME using Virus-Induced Gene Silencing (VIGS) and chemical treatments results in cytoplasmic effectors in swollen BICs lacking vesicles. In contrast, fluorescent marker co-localization, VIGS and chemical inhibitor studies failed to support a major role for clathrin-independent endocytosis in effector vesicle formation. Localization studies of two novel effectors, and of known effectors after CME inhibition, indicate that cytoplasmic effector translocation occurs underneath appressoria before invasive hyphal growth. Taken together, this study provides evidence that cytoplasmic effector translocation is mediated by clathrin-mediated endocytosis in BICs and suggests a role for *M. oryzae* effectors in co-opting plant endocytosis.

INTRODUCTION

Many filamentous eukaryotic plant pathogens, such as fungi and oomycetes, cause plant disease by hijacking and feeding on living plant cells, and they deliver effectors into and around host cells to promote infection (Giraldo and Valent, 2013; Lo Presti and Kahmann, 2017). This includes the Ascomycete fungus *Magnaporthe oryzae* (synonym of *Pyricularia oryzae*), which threatens global food security by causing blast diseases on rice, on several millets, and most recently on wheat (Gladieux et al., 2018; Valent et al., 2020). *M. oryzae* executes a hemibiotrophic lifestyle involving biotrophic invasion of successive plant cells by specialized intracellular invasive hyphae (IH) that grow from cell to cell (Kankanala et al., 2007). Blast IH growing in living host cells are enclosed by extensions of the plant plasma membrane termed the extra-invasive hyphal membrane (EIHM). Colonized cells die as they fill with hyphae and the EIHM and host vacuolar membranes become disrupted. Meanwhile, the fungus moves on to colonize neighboring cells using the same invasion strategy (Kankanala et al., 2007; Mochizuki et al., 2015; Sakulkoo et al., 2018; Jones et al., 2021).

57 Live cell imaging of blast IH invading optically clear rice leaf sheath cells has defined a
58 dimorphic hyphal switch associated with secretion and targeting of effectors – small, secreted
59 proteins that suppress immunity responses in host plant cells. Specifically, cytoplasmic effectors,
60 destined for translocation inside the host cell, are associated with the first two IH cells to grow in
61 the plant cell lumen, the tubular primary invasive hypha that grows directly after penetration and
62 the pseudohyphal bulbous IH cells that subsequently grow to fill the host cell (Kankanala et al.,
63 2007; Khang et al., 2010). Effectors destined for delivery to the host cytoplasm are secreted by a
64 specialized, Brefeldin A (BFA)-insensitive, Golgi-independent secretion system (Giraldo et al.,
65 2013). After secretion, these 'cytoplasmic effectors' accumulate in an extended dome-shaped
66 interfacial region of the EIHM matrix, the Biotrophic Interfacial Complex (BIC). BICs first occur
67 as 'tip-BICs' at primary hyphal tips, and then as 'side-BICs' that move beside the first bulbous IH
68 cell (Khang et al., 2010). During live cell imaging, fluorescent cytoplasmic effectors are routinely
69 detected in the cytoplasm and/or nuclei of invaded plant cells. Some cytoplasmic effectors are also
70 detected in the cytoplasm of surrounding plant cells, apparently moving through plasmodesmata
71 to prepare neighboring cells before invasion (Khang et al., 2010). In contrast, apoplastic effectors,
72 such as the biotrophy-associated secreted protein 4 (Bas4), the LysM protein 1 (Slp1), and Bas113,
73 are secreted via conventional Golgi-dependent secretion, and accumulate in the EIHM around the
74 entire IH (Giraldo et al., 2013). The retention of apoplastic effectors such as Bas4 inside the EIHM
75 (Mosquera et al., 2009; Khang et al., 2010), lack of separation of the EIHM from IH during
76 plasmolysis (Kankanala et al., 2007), and exclusion of the endocytosis tracker dye FM4-64 from
77 IH membranes inside the FM4-64 stained EIHM (Kankanala et al., 2007; Giraldo et al., 2013), all
78 indicate that IH grow inside a sealed EIHM compartment.
79 The mechanisms by which eukaryotic filamentous plant pathogens deliver effectors across
80 the host plasma membrane into living host cells are poorly understood, and may be conserved or
81 evolutionarily unique for different host-pathogen interactions (Giraldo and Valent, 2013; Petre and
82 Kamoun, 2014; Fawke et al., 2015; Lo Presti et al., 2015; Lo Presti and Kahmann, 2017). The
83 oomycete potato pathogen *Phytophthora infestans* resembles *M. oryzae* in having distinct secretion
84 systems for different classes of effectors. That is, cytoplasmic effectors are secreted by a Brefeldin
85 A (BFA)-insensitive (Golgi-independent) secretion and apoplastic effectors are secreted by
86 conventional BFA-sensitive secretion (Giraldo et al., 2013; Van den Ackerveken, 2017; Wang et
87 al., 2017). Although cell entry motifs for fungal effectors have not been identified, oomycete

effectors contain amino acid translocation motifs, with the RXLR motif being the most common. The RXLR motif in oomycete effectors was reported to mediate host cell uptake through endocytosis based on binding to phosphatidylinositol-3-phosphate (PI3P) in host membrane (Kale et al., 2010), although it was subsequently shown that the RXLR motif from *P. infestans* effector AVR3a is cleaved off before secretion from the pathogen (Wawra et al., 2017). Therefore, the function of RXLR motif in cell entry remains disputed (Petre and Kamoun, 2014; Trusch et al., 2018). Another amino acid motif, YKARK, appears involved in translocation of the effector SpHtp3 from *Saprolegnia parasitica*, a serious oomycete pathogen of fish, inside fish cells (Trusch et al., 2018). Specifically, this effector appears to be internalized inside host cells via lipid-raft mediated endocytosis through binding to a gp96-like receptor, and another effector is involved in releasing SpHtp3 from vesicles into the fish cytoplasm. In an example from a fungal pathogen, a solvent-exposed RGD vitronectin-like motif is required for internalization of ToxA, a host-specific proteinaceous toxin secreted by the necrotrophic wheat pathogen *Pyrenophora tritici-repentis* (Manning and Ciuffetti, 2005). In addition to uptake by plant endocytosis, effectors might enter plant cells through specialized translocon complexes in the plasma membrane. For example, the human malaria parasite, *Plasmodium falciparum*, is contained within a parasitophorous vacuole inside invaded red blood cells, and effectors are delivered across the membrane into the host cytoplasm by the PTEX translocon (Elsworth et al., 2014). Recently, a stable protein complex comprised of five unrelated fungal effectors and two fungal membrane proteins has been implicated in effector translocation by the maize smut fungus *Ustilago maydis* (Ludwig et al., 2021). However, the general question of how effectors are taken up into plant cells remains largely unresolved for eukaryotic plant pathogens.

Clathrin-mediated endocytosis (CME) is the major mechanism by which eukaryotic cells internalize extracellular or membrane-bound cargoes, and this process is best understood in mammalian systems and yeast (Kaksonen and Roux, 2018). Increasing understanding of CME in plants shows both conserved and evolutionarily unique mechanistic details (Qi et al., 2018; Reynolds et al., 2018; Dejonghe et al., 2019; Johnson et al., 2020; Narasimhan et al., 2020). CME is known to play key roles in plant-microbe interactions (Dodds and Rathjen, 2010; Beck et al., 2012; Fan et al., 2015). CME is required for immunity mediated by pattern recognition receptor kinases, for instance, specifically through internalization of activated extracellular pattern recognition receptors (PRRs) for degradation in the vacuole (Mbengue et al., 2016). Examples

119 include the pattern recognition receptor Pep receptor 1/2 (PEPR1/2), the EF-TU receptor (EFR)
120 recognizing the PAMP bacterial elongation factor, and FLS2 recognizing the PAMP flagellin (flg-
121 22) (Spallek et al., 2013; Mbengue et al., 2016), as well as the Cf-4 receptor-like protein that
122 recognizes the *C. fulvum* Avr4 avirulence effector (Postma et al., 2016). Trafficking of activated
123 PRRs requires clathrin and converges into endosomal vesicles that are also shared by the hormone
124 receptor Brassinosteriod Insensitive 1 (BRI1). Additionally, it is known that pathogens can control
125 plant CME. In addition to its role in suppressing INF1-mediated cell death, the *P. infestans* host-
126 translocated RXLR effector AVR3a was recently shown to associate with the Dynamin-Related
127 Protein 2, a plant GTPase implicated in receptor-mediated endocytosis, and to suppress flg22-
128 triggered defense responses and reduce FLS2 internalization (Chaparro-Garcia et al., 2015).
129 Therefore, AVR3a interacts with a membrane-remodeling complex involved in immune receptor-
130 mediated endocytosis. Also, in host cells containing haustoria from the oomycete *P. infestans*, the
131 late endosomal pathway is rerouted from the vacuole to the extrahaustorial membrane (EHM)
132 surrounding haustoria (Bozkurt et al., 2015). Multiple effectors from this pathogen are now
133 implicated in rerouting the host membrane trafficking system and autophagy machinery for the
134 benefit of the invading pathogen (Bozkurt et al., 2015; Dagdas et al., 2018; Petre et al., 2021).
135 Effector translocation in the *M. oryzae*/rice pathosystem can be assayed directly by live
136 cell imaging of fluorescently-labeled effector proteins inside host cells after secretion by IH
137 invading rice leaf sheath cells (Khang et al., 2010). Although some effectors naturally localize to
138 host nuclei, addition of a nuclear localization signal (NLS) to fluorescent effectors enhances
139 visualization of translocation and cell-to-cell movement. Blast cytoplasmic effectors apparently
140 do not contain a translocation motif as reported for oomycete effectors. Instead, preferential
141 accumulation in the BIC is the major predictor for translocation into the rice cell. Previously,
142 Nishizawa and colleagues reported that a cytoplasmic effector occurs in punctae (vesicles) in an
143 outer BIC region (Mochizuki et al., 2015; Nishimura et al., 2016; Nishizawa et al., 2016). Here,
144 we have used live-cell fluorescence imaging to characterize the nature and dynamics of membrane-
145 bound effector vesicles within BICs and in surrounding host cytoplasm. We show that BICs are
146 enriched for CME components, and we report functional analyses using virus-induced gene
147 silencing (VIGS) and pharmacological approaches. When considered together, our data indicate
148 that blast effectors are internalized through host clathrin-mediated endocytosis in the outer BIC
149 layers, followed by escape from the vesicles into the rice cytoplasm.

150

151 **RESULTS**

152

153 **BICs contain multiple vesicles labeled by cytoplasmic effectors**

154 BICs were previously reported as interfacial structures containing fluorescently-labelled
155 apoplastic effectors, such as Bas4:eGFP, in an inner base layer and a concentration of fluorescent
156 cytoplasmic effectors in the outer 'dome-shaped' region (Khang et al., 2010; Nishizawa et al.,
157 2016). Using laser confocal imaging, we now routinely resolve the dome region of BICs as a
158 concentration of vesicles containing fluorescent cytoplasmic effectors (Figure 1). These effector
159 vesicles are illustrated by an image of a BIC at the tip of a primary hypha (tip-BIC) expressing
160 fluorescent apoplastic effector Bas4:eGFP and fluorescent cytoplasmic effector Pwl2:mRFP
161 (Figure 1A). The Bas4:eGFP fluorescence remains distributed throughout the EIHM matrix
162 surrounding the entire growing IH, including in an inner layer of the BIC. In contrast, Pwl2:mRFP
163 occurs as distinct vesicles in the outer BIC region. We have observed effector vesicles in tip-BICs
164 labeled with additional translocated effectors Bas1 and Pwl1 fused to either eGFP or mRFP
165 (Supplemental Figure S1). Vesicles are also observed after tip-BICs move beside the first bulbous
166 IH cells (side-BICs) (Figure 1B; Supplemental Figure S2). We evaluated the proximity of these
167 vesicles relative to both tip- and side-BICs. Whereas the vast majority of vesicles associated with
168 primary IH were located in the tip-BIC, some vesicles associated with side-BICs were found in
169 regions of the cytoplasm at least 7 µm from the fungal cell wall at the BIC, which we define as
170 outside the BIC (Figure 1C). Inclusion of the apoplastic effector Bas4:eGFP in these experiments
171 confirmed that the EIHM remained intact at each infection site, based on its uniform outlining of
172 the IH and lack of spilling into the invaded rice cell.

173 We identified a novel cytoplasmic effector, Bas170 (MGG_07348.6), with amino acid
174 sequence similarity to previously identified effector Bas83 (Mosquera et al. 2010; Supplemental
175 Figure S3). Unlike previous cytoplasmic effectors including Pwl2, Pwl1, and Bas1, fluorescent
176 Bas170 fusion proteins localized in vesicles in the rice cytoplasm short distances from the
177 appressorial penetration site at a stage even before visible primary hyphal growth (Figure 1D and
178 F). The Bas170:mRFP fusion protein naturally accumulates in the rice nucleus at this early
179 infection stage, presumably to reprogram plant transcription essential for infection (Figure 1D and
180 F). These results suggest rapid effector translocation from appressoria even before growth of
181 primary IH. Bas170:mRFP also labels BIC-associated vesicles in tip-BICs and side BICs after

182 growth of IH in the cell. The vesicular BIC-localization pattern of fluorescent Bas170 was similar
183 to BIC-localization patterns of Pwl2-, Pwl1- and Bas1-fusion proteins (Figure 1E,F), but these
184 latter effectors have not been observed under appressoria at the earlier time period.

185 **Vesicles in BICs are dynamic through time**

186 To understand vesicle dynamics in BICs through time, we imaged BIC effector fluorescence
187 during the morphogenic switch from tubular primary hyphae to bulbous IH using a strain co-
188 expressing two cytoplasmic effectors, Bas1:eYFP and Pwl2:mRFP (Figure 2). The vesicle content
189 varied over the 2-hour period when the tip-BIC was displaced from the primary hyphal tip to
190 become a side-BIC beside the differentiating bulbous IH cell. In early stage tip-BICs, fluorescence
191 from these two effectors often appeared to be sorted into different vesicles. For this series of
192 experiments, Pwl2:mRFP occurred in vesicles that reached outer layers of the tip-BIC compared
193 to Bas1:eYFP. Pwl2:mRFP appeared less abundant relative to Bas1:eYFP during the switch from
194 tip- to side-BIC, recovering again after growth of bulbous IH (Figure 2A). Both vesicle size and
195 content vary within BICs through time (Figure 2 B-F). Specifically, BICs at primary hyphal tips
196 contain a larger number of smaller vesicles (Figure 2D,E). Whereas BICs on primary hyphae
197 contain effectors in vesicles with a median diameter of 249 nm, BICs on mature bulbous hypha
198 contain effectors in larger vesicles with a median diameter of 647 nm, ranging from ~500 nm up
199 to above 1000 nm at later cell colonization stages (Figure 2C,D). Larger effector vesicles beside
200 mature bulbous IH often showed colocalization of fluorescence from different effectors compared
201 to vesicles in tip-BICs (Figure 2A, B and F).

202 Cytoplasmic connections were observed between BICs and plant cytoplasm at the
203 periphery of the invaded cell, illustrated in optical sections through a BIC in Supplemental Movie
204 S1. This is consistent with a previous report of dynamic connections linking BICs and host
205 cytoplasm underneath the appressorium (Khang et al., 2010). These cytoplasmic connections may
206 facilitate movement of effectors from cytoplasm surrounding the BIC in the cell center to the
207 peripheral cytoplasm, in position to rapidly move through plasmodesmata into neighboring cells.

208 **BIC vesicles are surrounded by plant plasma membrane**

209 We previously reported that BICs are enriched in plant plasma membrane based on infection of
210 transgenic rice expressing a plasma membrane marker (Giraldo et al., 2013). Here we use rice lines
211 expressing LTi6B:GFP to confirm colocalization of plant plasma membrane and vesicles in BICs

212 (Figure 3A,B). Individual effector vesicles were observed to be surrounded by labeled plant plasma
213 membrane (Figure 3C), especially for vesicles in side-BICs on mature bulbous hyphae, where the
214 vesicles reach diameters of 500 nm or larger.

215 To further confirm that BIC vesicles are associated with plant membrane, we evaluated
216 BIC membrane composition by staining with the endocytosis tracker dyes FM4-64 and FM1-43
217 (Figure 3D,E). These amphiphilic styryl dyes insert in the plasma membrane where they diffuse
218 laterally in plant and fungal membranes and are internalized into cells via endocytosis (Atkinson
219 et al., 2002; Bolte et al., 2004). For healthy IH growing in rice cells, FM4-64 heavily stains the
220 EIHM surrounding IH, but is excluded from IH membranes inside the EIHM compartment
221 (Kankanala et al., 2007; Giraldo et al., 2013). This is clearly visualized by lack of lateral diffusion
222 into IH septal membranes and lack of accumulation in IH vacuolar membranes (Giraldo et al.,
223 2013; Kankanala et al., 2007). In these experiments, exclusion of FM4-64 or FM1-43 staining
224 from internal IH membranes served as a control for EIHM intactness at observed infection sites
225 (Figure 3D and Supplementary Movie S2). Quantification of FM4-64 and FM1-43 accumulation
226 in both tip- and side-BICs (Figure 3E) confirmed that effector vesicles were immersed in the region
227 of intense dye staining (Figure 3D; Supplementary Movie S2). Vesicles that carry effectors were
228 infrequently observed separated from the BIC by at least 7 µm (Figure 3D left, right; Supplemental
229 Movie S2). Apparent vesicular bursting was also observed, which suggests that the vesicles are
230 unstable, presumably releasing the effector contents into the host cytoplasm. Taken together,
231 results from labeling of rice plasma membrane with both LTi6B:GFP membrane fusion protein
232 and endocytosis tracer dyes are consistent with the formation of BIC-associated effector vesicles
233 through plant endocytosis.

234 **Cytoplasmic effector Bas83 associates with rice membrane vesicles concentrated around**
235 **BICs**

236 Since it is likely that specific blast effectors play roles in vesicle formation and effector
237 translocation, we were particularly interested in effectors that appear to associate with membranes
238 in host cells. The *BAS83* (MGG_08506.6) gene is unique to *M. oryzae*, and it is 36-fold upregulated
239 during biotrophic invasion (Mosquera et al., 2009). Bas83:mRFP is translocated into invaded host
240 cells, but it does not precisely colocalize with other BIC-localized cytoplasmic effectors
241 Pwl2:eGFP and Pwl1:eGFP (Figure 4A; Supplemental Figure S4). In contrast, Bas83:mRFP seems
242 to label the EIHM surrounding the BIC-associated cells, the primary hyphae and first bulbous IH,

243 and it labels bubbles, or vesicles, near to BICs and BIC-associated cells (Figure 4A-C). Figure 4A
244 shows that Bas83:mRFP-labeled vesicles do not contain the cytoplasmic effector Pwl2:eGFP,
245 indicating they are distinct from effector vesicles in BICs. Bas83:mRFP is also associated with
246 vesicles observed under appressoria (Figure 4C; Supplemental Figure S4). However, Bas83:mRFP
247 fails to label membrane surrounding subsequently formed bulbous IH that are associated with
248 apoplastic effectors and not with cytoplasmic effectors (see 2nd bulbous IH in Figure 4C). We
249 hypothesize that Bas83 is involved in recruiting new plant plasma membrane to form the EIHM
250 and BICs during biotrophic development. However, repeated attempts in two different laboratories
251 (264 purified transformants, 4 methods and 5 experiments; KSU and Univ. of Exeter) failed to
252 produce knock-out mutants for further functional analysis (Supplemental Figure S5).

253 **BICs contain plant actin**

254 Although it is now clear that actin is dispensable for CME vesicle formation at the plasma
255 membrane in plant cells, actin filaments likely play a role in short-distance movement of
256 internalized vesicles (Narasimham et al., 2020; Ruan et. al., 2021: Schuh, 2011). Therefore, we
257 localized plant actin during biotrophic invasion using rice lines expressing the actin marker
258 LifeAct:eGFP. Infection by *M. oryzae* strains expressing chimeric protein Pwl2:mRFP showed
259 localization of LifeAct:eGFP at BICs (Figure 5A). Actin was abundant in all imaged tip- and side-
260 BICs (Figure 5B). Likewise, colocalization of fluorescent Phalloidin conjugates and fluorescently-
261 labeled effector confirmed that BICs are rich in plant actin filaments (Figure 5C). We hypothesize
262 that actin filaments are responsible for the transport of effector vesicles in the rice cell cytoplasm.

263 **BICs consistently contain plant clathrin**

264 Clathrin-mediated endocytosis (CME) is the major endocytosis mechanism in plants, with some
265 contribution by Clathrin-independent endocytosis (CIE) (Chen et al., 2011; Ewers and Helenius,
266 2011; Fan et al., 2015; Narasimhan et al., 2020). To assess localization of specific endocytosis
267 markers in BICs, we generated transgenic rice lines expressing a fluorescent marker for either
268 CME or CIE. For CME, we generated a C-terminal translational fusion of eGFP with the rice
269 clathrin light chain-1 (OsCLC1), which is a component of the clathrin coat together with the
270 clathrin heavy chain. Rice lines expressing OsCLC1:eGFP show typical clathrin foci (Konopka et
271 al., 2008; Narasimhan et al., 2020) in uninfected rice cells (Figure 6). The marker for CIE was a
272 C-terminal translational fusion of eGFP to Flotillin-1 (Flot1), which is a component of lipid rafts

273 (Otto and Nichols, 2011; Li et al., 2012). Rice lines with the CME and CIE markers were used for
274 leaf sheath assays with an *M. oryzae* strain expressing Pwl2:mRFP to label BICs. In addition to
275 typical clathrin foci around the cell periphery, all tip-BICs and side-BICs contain fluorescence
276 from OsCLC1:eGFP co-localizing with Pwl2:mRFP (Figure 6A,B and E). Indeed, clathrin
277 fluorescence was observed co-localizing with Pwl2:mRFP or Bas1:mRFP effector fluorescence in
278 BIC vesicles in both tip and side-BICs (Figure 6A-C; Supplemental Figure S6; Supplemental
279 Movie S3). In contrast, very few (~4%) tip-BICs colocalized with Flot1:eGFP. Some
280 colocalization of Flot1:eGFP and Pwl2:mRFP occurred in side-BICs besides mature bulbous
281 hyphae (Figure 6D,E). Colocalization results from several independent experiments were
282 consistent with a major role for CME, but not for CIE, in the internalization of cytoplasmic
283 effectors.

284 **Silencing of rice endocytosis machinery blocks *M. oryzae* infection and impacts BIC structure**
285 We assessed the impact of inhibition of CME and CIE on BICs and effector vesicles using the
286 brome mosaic virus system (Ding et al., 2006; Ding et al., 2007) for silencing of genes for CME
287 and CIE components previously characterized in *Arabidopsis*. Specifically, we silenced two rice
288 CME genes, Adaptor protein complex-2 subunit α2 (*AP-2*α) and clathrin heavy chain-1 (*CHC1*)
289 (Di Rubbo et al., 2013; Larsson et al., 2017) as well as the CIE gene *Flotillin-1* (*Flot1*) (Li et al.,
290 2012). Silencing of both CME components *AP-2*α and *CHC1* resulted in severe reduction in
291 pathogenicity in whole plant spray inoculation assays (Figure 7A,B). However, as expected,
292 silencing of these genes caused stunting and decreased plant health (Supplemental Figure S7), and
293 levels of pathogenicity in blast disease are known to be decreased on unhealthy rice plants. More
294 significant is the phenotype of pathogen blockage at individual infection sites. Silencing of either
295 CME component RNAi*AP-2*α or RNAi*CHC1* led to a distinctive swollen BIC phenotype, with
296 enlarged, abnormally-shaped BICs that lack effector vesicles (Figure 7C-F). The swollen BIC
297 phenotype would be consistent with effectors still being secreted by the fungus, but remaining
298 trapped within the EIHM due to blocking of CME. By contrast, silencing of the CIE marker gene
299 *Flot1* showed less severe stunting (Supplemental Figure S7), less of an impact on pathogenicity
300 (Figure 7A,B), and minor impact, if any, on BIC structure (Figure 7C-F). For example, compare
301 the 28 hours post-inoculation (hpi) images of BICs in control rice plants with the RNAi*Flot1*-
302 silenced and the RNAi*AP-2*α-silenced rice plants in Figure 7C, and quantification of swollen BIC
303 events in Figure 7F.

304 In addition to swollen BICs at sites with primary hyphae, silencing of both CME genes
305 decreased appressorial penetration and induced the accumulation of the cytoplasmic effector
306 Pwl2:mRFP under failed penetration sites, where it is not normally observed (Figure 7 C-
307 18hpi,D,E). In contrast, silencing of *Flot1* had only minor effects on appressorium penetration and
308 on accumulation of Pwl2:mRFP under failed appressoria. Similar to our finding of early
309 accumulation of Bas170 under appressoria before penetration, these results again suggest that
310 effector uptake begins before host penetration. These results also suggest that CME plays a role in
311 effector translocation at the appressorial penetration stage as well as from BICs.

312 **Chemical inhibition of rice endocytosis machinery blocks *M. oryzae* infection**

313 Pharmacological approaches have impacted studies in diverse biological systems (Robinson et al.,
314 2008; Hicks and Raikhel, 2010; Grassart et al., 2014; Fan et al., 2015). To further assess potential
315 impact of the plant endocytic machinery on cytoplasmic effector translocation, we tested a series
316 of chemicals that are reported to inhibit plant CME or CIE (Table 1). Compared with the non-
317 treated control (Figure 8A), treatment with CME inhibitor Endosidin9-17 (ES9-17), which directly
318 inhibits clathrin heavy chain function in both *Arabidopsis* and human cells (Dejonghe, et al., 2019),
319 led to abnormally-shaped swollen BICs that lack distinct effector vesicles, resembling those seen
320 with silencing of CME components CHC-1 and *AP-2*α (Figure 8B). Treatment with cantharidin,
321 which is reported to inhibit signaling associated with CME, also produced swollen BICs lacking
322 effector vesicles (Figure 8C). Fluorescence intensity linescans confirm that ES9-17 and
323 cantharidin had little, if any, impact on localization of apoplastic effector Bas4:eGFP in the base
324 of the BIC (Figure 8).

325 We quantified Pwl2:mRFP localization patterns during infection of rice with no treatment,
326 after treatment with five chemicals reported to impact CME inhibitors, two chemicals reported to
327 impact CIE, and 2 chemicals with less defined roles in inhibiting endocytosis (Figure 9). The five
328 CME inhibitors included ES9-17 and cantharidin (Figure 8) along with additional reported CME
329 inhibitors, Endosidin9 (ES9), chlorpromazine and triclosan (Table 1). Compared to the untreated
330 control, each of these five CME-associated inhibitors showed a high proportion of swollen,
331 irregular-shaped cytoplasmic effector fluorescence patterns in BICs (Figure 9A-C). By contrast,
332 inhibition of CIE with filipin and methyl-β-cyclodextrin resulted in minor to no effect on BIC
333 effector fluorescence patterns (Figure 9A-C), which was consistent with results from silencing of
334 CIE (Figure 8). Two chemical inhibitors with potential CME association (Table 1) show different

335 impacts on BIC effector fluorescence patterns. Wortmannin, which inhibits phosphatidylinositol
336 3-kinase (PI 3-kinase) and is implicated in late endosomal trafficking (Robinson et al., 2008) gave
337 the swollen BIC phenotype, while concanamycin A, which inhibits vacuolar-type ATPase and
338 induces vacuolar acidification (Robinson et al., 2008), had little impact on BIC structure (Figure
339 9A-C).

340 Moreover, treatment with inhibitors associated with CME, triclosan, cantharidin,
341 chlorpromazine, ES9, and ES9-17, but not with inhibitors associated with CIE, filipin and methyl-
342 β-cyclodextrin, resulted in reduced appressorial penetration and induced abnormal accumulation
343 of the cytoplasmic effector Pwl2:mRFP under appressorial penetration sites where it is not
344 normally observed (Figure 9A - compare 18 hpi CIE and CME inhibitors; Figure 9D,E).
345 Wortmannin, which produces swollen BICs, also impacted appressorial function and resulted in
346 abnormal Pwl2:mRFP accumulation under appressoria (Figure 9D,E). Concanamycin A produced
347 none of the CME-associated phenotypes (Figure 9). Therefore, chemical inhibition of endocytosis
348 in rice cells undergoing *M. oryzae* infection mimics the results obtained with VIGS, further
349 supporting a role for CME in effector uptake into rice cells. These CME inhibition results support
350 our findings with Bas170:mRFP (Figure 1D-F) in suggesting that effector uptake begins before or
351 at the point that host penetration occurs.

352

353 **DISCUSSION**

354 Our results, when taken together, provide strong evidence that cytoplasmic effector translocation
355 is BIC-localized and mediated by clathrin-mediated endocytosis (CME). We report that BICs
356 contain multiple hallmarks of active CME. Specifically, BICs uniformly show focal accumulation
357 of fluorescently-labeled Clathrin Light Chain-1 (CLC1:eGFP), a key subunit of the clathrin coat
358 in CME (Figure 6). Indeed, CLC1:eGFP fluorescence has frequently been observed in a pattern
359 co-localizing with individual cytoplasmic effector vesicles (Figure 6A and B; Supplemental Figure
360 S6; Supplemental Movie S3). Fluorescent rice plasma membrane fusion protein LTi6B:eGFP
361 colocalizes with effector vesicles (Figure 3C, Supplemental Movie S2). Results with endocytosis
362 tracer dyes FM4-64 or FM1-43 served both as a control that the EIHM was intact and excluding
363 the dye from reaching fungal membranes at imaged infection sites (Kananala et al., 2007; Giraldo
364 et al., 2013), and showed effector vesicles emersed in stained plant membranes (Figure 3D and E).
365 Functional analyses via virus induced gene silencing of two rice CME components, Clathrin Heavy

366 Chain-1 (CHC-1) and Adaptor Protein Complex subunit 2α (AP-2α) decreased pathogenicity and
367 resulted in a 'swollen BIC' phenotype in which cytoplasmic effectors appear retained inside an
368 enlarged BIC compartment lacking distinct vesicles (Figure 7). In contrast, parallel experiments
369 showed that fluorescently-labeled clathrin independent endocytosis (CIE) component Flotillin-1
370 (Flot1:eGFP) rarely localized at BICs, and silencing of Flotillin-1 had minimal effects on BIC
371 vesicular structure (Figure 7). Additionally, treatment with 6 different pharmacological agents
372 associated with CME, including the direct inhibitor of clathrin heavy chain function Endosidin9-
373 17, resulted in the swollen BIC phenotype. Parallel experiments with pharmacological inhibitors
374 associated with CIE show little or no impact on BIC vesicular structure and pathogenicity (Figure
375 8 and 9). Taken together, our results therefore provide evidence that BICs include a focused region
376 of plant clathrin-mediated endocytosis for internalizing cytoplasmic effectors inside living plant
377 cells (Figure 10).

378 Both VIGS and pharmacological inhibitor strategies have potential interpretation
379 problems. Rice plants that received the CHC-1 and APC-2 silencing vectors were significantly
380 reduced in rice blast symptoms, compared to the empty vector control and to Flot1-silenced lines
381 (Figure 7; Supplemental Figure S7). However, this could be due, at least in part, to inevitable
382 health costs to the plant through silencing component genes for essential cellular processes.
383 Unhealthy rice plants are generally less susceptible to blast disease (Kato, 1974). Additionally,
384 care must be taken in the interpretation of results in pharmacological studies based on new
385 evidence that endocytosis inhibitors characterized in mammalian systems may not have the same
386 targets in plants (Dejonghe et al., 2016; Dejonghe et al., 2019), and pharmacological agents also
387 have off-target effects (Hicks and Raikhel, 2010; Dutta and Donaldson, 2012; Dejonghe and
388 Russinova, 2017). However, the consistent swollen BIC phenotype, seen only with treatments that
389 inhibit CME and consistent with trapping of cytoplasmic effectors inside the BIC (Figures 7-9),
390 lends credibility to our interpretation of these results. Our results do not rule out a minor role for
391 CIE in effector translocation because CIE inhibition has some impact. It remains to be determined
392 if this impact is due to some minor role for CIE or to the reported minor impact of CIE inhibitors
393 filipin and methyl-ß-cyclodextrin on CME (Rodale et al., 1999; Dutta and Donaldson, 2012).

394 We report that sizes and content of effector vesicles are dynamic through time as host cell
395 invasion progresses. At our levels of resolution, effector vesicles are relatively smaller (median
396 diameter 249 nm) in tip-BICs and increase in size (median diameter 647 nm) especially in later

397 stage side-BICs (Figure 2D). These results confirm and expand on a previous report that
398 cytoplasmic effectors occur in ~500 nm vesicles in the outer BIC domes beside bulbous IH
399 (Mochizuki et al., 2015; Nishimura et al., 2016; Nishizawa et al., 2016). It is unknown why these
400 pathogen-induced effector vesicles have so much larger diameters than reported for plant clathrin
401 coated vesicles (CCVs), which have mean diameters of 59.1 nm for the pentagonal basket
402 population, of 66.1 nm for the hexagonal basket population, and of 85 nm for the irregularly
403 ordered basket population (Narasimhan et al., 2020). The clear increase in effector vesicle sizes
404 through time could be due to biogenesis of larger vesicles, or to aggregation and/or fusion of
405 effector vesicles. Narasimhan et al. (2020) report that Arabidopsis CCVs show delayed and
406 sequential uncoating, and they present evidence for aggregated, partially fused CCVs associated
407 with internal membranes. Future research should explore the differences and similarities in the
408 biology of effector vesicles and normal plant CCVs.

409 We have identified additional factors that may play a role in effector translocation. We
410 report accumulation of actin in the BICs, as detected in stable transgenic plants expressing
411 LifeAct:eGFP and by staining with rhodamine-labeled phalloidin (Figure 5). It was recently
412 reported that actin is not required for internalization of clathrin-coated vesicles in plants as it is in
413 the well-studied systems in mammals and yeast (Qi et al., 2018; Johnson et al., 2020; Narasimhan
414 et al., 2020). Although a role for actin in plant endocytosis is unknown, actin filaments may be
415 involved in movement of vesicles and cargo sorting after internalization. We hypothesize that actin
416 filaments may be involved in short-distance transport of effector vesicles in the rice cell cytoplasm.
417 Additionally, we identified a novel effector, Bas83, that labels non-effector vesicles and EIHM
418 focused around BICs and the BIC-associated cells. Future research will determine if Bas83 could
419 play a role in replenishing host membranes needed for extensive endocytotic activity in the BIC
420 (Figure 4; Supplemental Figure S4).

421 We report two new lines of evidence that effectors are being secreted and translocated into
422 the host cytoplasm from appressoria even before obvious growth of primary hyphae inside host
423 cells. First, we identified an effector, Bas170, that naturally accumulates in host nuclei before
424 visible growth of primary hyphae, and it also localizes to vesicles underneath appressoria at this
425 early time point. Second, effector Pwl2:mRFP, which is not normally observed before the tip-BIC
426 stage, accumulates under appressoria that failed to penetrate after both VIGS silencing and
427 chemical inhibition of rice CME. These new findings are consistent with reports that rice cells

428 recognize and respond to *M. oryzae* before and independently of appressorial penetration (Xu et
429 al., 1998). It has been predicted that *M. oryzae* appressorial pores, a transient cell wall-less region
430 of the appressorium adjacent to the plant cuticle, might be involved in molecular communication
431 between pathogen and host before penetration (Howard and Valent, 1996). Previously, the only
432 *M. oryzae* effector that was a candidate for secretion through the appressorial pore was a presumed
433 secondary metabolite that is produced by the *AVR* gene *ACE1* encoding a hybrid polyketide
434 synthase (PKS) and nonribosomal peptide synthetase (NRPS) that is specifically expressed in the
435 cytoplasm of appressoria before and during penetration (Fudal et al., 2007; Collemare et al., 2008).
436 Therefore, our new effector localization results suggest similar exquisite staging of effector
437 expression as reported for the crucifer pathogen *Colletotrichum higginsianum*, which secretes
438 ChEC effectors under the appressorial pores and at subsequent stages during the invasion of
439 *Arabidopsis thaliana* cells (Kleemann et al., 2012). Specifically, this fungus focally secreted
440 effectors Chec6 and Chec36 from the appressorium pore, suggesting these effectors may be
441 translocated before fungal penetration (Kleemann et al., 2012). Our results with Bas170 together
442 with ChECs and Ace1 protein localization patterns indicate that many effectors might be focally
443 secreted through appressorial pores (Fudal et al., 2007; Kleemann et al., 2012), highlighting a
444 potential role for fungal appressoria in effector delivery. Recently, Yan et al. (2022) classified 10
445 modules of temporally co-expressed genes ranging from 0 hpi to 144 hpi, including some localized
446 to the appressorial pore, among 546 predicted MEP (*Magnaporthe* effector protein) genes.

447 The effector vesicle dynamics that we report support the idea that front-loaded effector
448 translocation occurs during the early stages of host cell invasion. Specifically, tip-BIC vesicles are
449 relatively small, abundant and selective in terms of sorting different cytoplasmic effectors,
450 Bas1:eYFP and Pwl2:mRFP, into different vesicles. In contrast, side-BICs contain fewer, larger,
451 less-selective vesicles that frequently contain both Bas1:eYFP and Pwl2:mRFP. Effector vesicles
452 observed in the cytoplasm were almost uniformly found at the side-BIC stage, perhaps indicating
453 a slow-down of the mechanism for effector release from the vesicles as BICs mature. Indeed, rare
454 very large vesicles can be seen in some host cells at later stages of invasion (Figure 2C). The
455 mechanism for forming vesicles may result in larger vesicles, or vesicles may fuse before releasing
456 effectors to the cytoplasm in the later BIC stages. Slowdown of the translocation system would
457 appear consistent with previous reports of loss of activity in BICs as host cells fill with IH (Khang
458 et al., 2010; Jones et al., 2021). Front-loading effector translocation from BICs would make sense

459 because cell-to-cell movement of blast cytoplasmic effectors through plasmodesmata must occur
460 in the early stages of host cell invasion while the EIHM enclosing the IH remains intact and
461 plasmodesmata in the invaded cell remain open (Sakulkoo et al., 2018; Jones et al., 2021). Active
462 BICs are surrounded by host cytoplasm with dynamic connections to the cell periphery (Khang et
463 al., 2010; Supplemental Movie S1), where cytoplasmic streaming would rapidly disperse effectors
464 to pit fields containing plasmodesmata. In contrast, nonBIC-associated IH cells invaginate the host
465 vacuole and grow in close proximity to the host vacuolar membrane with little surrounding
466 cytoplasm (Mochizuki et al., 2015; Jones et al., 2021). Specifically, the host vacuole remains
467 intact, but shrinks as IH grow. Both the EIHM and vacuolar membrane become disrupted,
468 indicating death of the invaded cell, around the time IH move into neighboring cells to repeat their
469 BIC-mediated invasion strategy (Mochizuki et al., 2015; Jones et al., 2021).

470 There is evidence supporting occurrence of clathrin-mediated endocytosis at the EHM in
471 one additional pathosystem. That is, transmission electron micrographs of the interfacial matrix
472 between the intracellular hyphae [called monokaryotic (M)-haustoria] of the monokaryotic rust
473 fungus *Uromyces vignae* and its host cowpea (*Vigna unguiculata*) shows clathrin-coated pits
474 (diameter ca. 50-70nm) on the EHM at M-haustoria hyphal tips that contained dense cytoplasm
475 and were presumably growing (Stark-Urnau and Mendgen, 1995). The coated vesicles were
476 labeled by an antibody recognizing the clathrin heavy chain subunit. Long tubules extending into
477 the host cytoplasm, as well as coated vesicles in the surrounding host cytoplasm, were also labeled
478 with the antibody, indicating that endocytosis occurs at the EHM (Stark-Urnau and Mendgen,
479 1995; O'Connell and Panstruga, 2006). It was suggested that these endocytic vesicles might be
480 involved in effector uptake into host cells in addition to membrane recycling from host exocytosis.
481 Unfortunately, lack of transformation capability and identification of effectors makes it difficult
482 to follow up on these intriguing results with *U. vignae*. Additional TEM studies support our results
483 that transient silencing of lipid raft-mediated endocytosis component Flotilin1, as well as filipin
484 treatment, had little effect on BIC structure and effector vesicle formation. Freeze-fracture
485 transmission electron microscopy (TEM) following filipin treatment revealed an absence of
486 granular filipin-sterol complexes on the EHM of two rust fungi, *Puccinia coronata* and *Uromyces*
487 *appendiculatus* (Harder and Mendgen, 1982), suggesting that the extrahaustorial membrane
488 contains less sterol than normal plasma membranes, and indicating that the EHM appears depleted
489 in sterol-rich lipid rafts.

490 Differences in infection strategies among various filamentous biotrophic or hemibiotrophic
491 pathogens would be consistent with use of different strategies for effector translocation in different
492 pathosystems. A recent report indicates that a complex of seven proteins from the smut pathogen
493 *U. maydis* is critical for infection and implicated in translocation of cytoplasmic effectors into
494 maize cells (Ludwig et al., 2021). This basidiomycete fungus colonizes host tissue as intracellular
495 hyphae that pass through and between host cells without obviously specialized interfacial zones,
496 and fluorescent fusion proteins of cytoplasmic effectors have not been visualized in the host cell
497 cytoplasm in this pathosystem (Lo Presti et al., 2017). *U. maydis* produces galls on maize seedlings
498 and grows systemically as the plant grows to finally invade ovaries, which swell into dramatic
499 sporulating galls. In contrast, *M. oryzae* densely colonizes a localized tissue area that will become
500 a visible eyespot lesion that releases spores to reinitiate the infection cycle within 7 days. Different
501 pathogenic lifestyles could present different demands for cytoplasmic effector translocation.
502 Taken together, our data strongly suggest that clathrin-mediated endocytosis occurring in
503 BICs is a key mechanism for internalization of *M. oryzae* effectors inside living rice cells,
504 beginning even before appressorium penetration of the host surface. Further confirmation will
505 come through continuing research to determine how the endocytic machinery is recruited to BICs
506 and how it interacts with effector cargos (Qi et al., 2018). It is important to understand if, and if
507 so, how, Bas83 contributes to membrane recruitment to BICs and the EIHM surrounding BIC-
508 associated cells. It is of interest to understand how supposedly coordinately-expressed effectors
509 Bas1:eYFP and Pwl2:mRFP can be sorted into different effector vesicles, as seen in Figure 2A. It
510 is important to understand vesicle dynamics, including and why effector vesicles become larger
511 and more persistent as BICs mature, and why effector vesicles are more easily observed in the host
512 cytoplasm near-by maturing side-BICs (Figure 2). Identification of effectors with critical roles in
513 the translocation process is a high priority, including effectors that are involved in disrupting
514 effector vesicles and releasing effectors into the rice cytoplasm. It is important to understand the
515 role for appressoria in effector secretion before penetration, and how these early effectors, such as
516 the host nuclear localized effector Bas170, function to promote infection. Finally, it is critical to
517 translate molecular mechanisms of blast biotrophic invasion into strategies for controlling
518 devastating diseases on rice, wheat and other food crops worldwide.
519
520

521 **METHODS**

522 **Live-cell imaging of *M. oryzae* effectors *in planta***

523 Fungal strains were stored in dried filter papers at -20˚C, and cultured on rice polish agar plates at
524 25˚C under continuous light for 2 weeks (Valent and Chumley, 1991). Rice sheath inoculations
525 were performed as described (Kankanala et al., 2007) with the following modification. We used
526 sheath pieces that were thickly trimmed (~7 rice cell layers thick) compared to thinner trimmed
527 sheaths (~3 cell layers thick) in previous publications. Brightfield images were less detailed, but
528 the endocytic machinery appeared more active, providing enhanced microscopic resolution of
529 fluorescent marker dynamics. Susceptible rice variety YT-16 was used unless mentioned
530 otherwise. Briefly, 7-cm-long sheath pieces from 3-week-old plants were placed in a sealable
531 Pyrex glass moist chamber. Leaf sheath sections were placed on inverted 8-well PCR tube strips
532 to avoid contact with wet paper and to hold epidermal cells directly above the mid-vein
533 horizontally flat for uniform inoculum distribution in the trimmed sheath pieces (Oliveira and
534 Valent, 2021). A spore suspension (10^4 spores/ml in sterile 0.25% gelatin, Cat. #G-6650, Sigma-
535 Aldrich) was prepared from 10-day old cultures and was injected into one end of the sheath using
536 a 100-ml pipette. Each segment was trimmed at 18–30 h.p.i., treated with specific dyes or
537 inhibitors, or imaged immediately by laser confocal microscopy. Biological replicates were
538 independent experiments performed with fungal cultures fresh out of frozen storage and with new
539 rice plants. All conclusions are supported by at least 3 biological reps, with each replication
540 including observation of around 100 infection sites.

541 Confocal imaging was performed with a Zeiss LSM780 confocal microscope system using
542 two water immersion objectives, C-Apochromat 40x/1.2 WCorr. and C-Apochromat
543 63x/1.2WCorr. Excitation/emission wavelengths were 488 nm/505–550 nm for eGFP and FM1-
544 43, and 543 nm/560–615 nm for mRFP, mCherry, Phalloidin and FM4-64. Image acquisition and
545 processing, some vesicle quantification, and fluorescence intensity linescans were done using
546 Zeiss ZEN 2010 software. Images of effector vesicles in Figure 3C were obtained using a Leica
547 SP8 confocal microscope system with a water immersion objective HC PL APO 63x/1.20 WCorr.
548 Excitation/emission wavelengths were 488 nm/505–550 nm for eGFP and 543 nm/560–615 nm
549 for mRFP. Leica SP8 software at the University of Exeter and at the Lousiana State University

550 Agricultural Center were used for some vesicle quantification and for analyzing ES9 and ES9-17
551 CME inhibitor assays.

552 **Size measurements of vesicles carrying effector and clathrin fluorescence**

553 To measure BIC vesicle sizes, high resolution confocal microscopy images of BICs were generated
554 from infected YT16 rice undergoing infection of *M. oryzae* strains KV170 or KV209 expressing
555 Bas1:mRFP or Pwl2:mRFP, respectively. We began with maximum intensity projections of Z-
556 stack image series of BICs obtained with the Zeiss and Leica confocal microscopes. However,
557 when vesicles were too close in the collapsed images, distinction between two or more vesicles
558 was attempted using individual images in the Z-stack. For example, see Supplemental Movie S3.
559 Scale bars were set to 1 µm. Amplified images were opened in ImageJ (Schneider et.al., 2012) and
560 distances in pixels was correlated to the 1 µm (1000nm) scale bars. Vesicle diameters were
561 measured using the length measurement tool. Data was exported in Excel and analyzed using the
562 Prism 9 software.

563 **Fungal strains, DNA manipulation, and fungal transformation**

564 *Magnaporthe oryzae* wild type strain Guy11, a field isolate from rice in French Guiana, was
565 obtained from J.L. Notteghem (Centre de Cooperation Internationale en Recherche Agronomique
566 pour le Developpment, France). *M. oryzae* transformants are described in Supplemental Table S1
567 online. Effector:mRFP and Effector:eGFP expression plasmids were constructed by PCR
568 amplifying different effector gene regions and fusing them to the N-terminus of mRFP and eGFP,
569 respectively. Details of construction of each plasmid are described in Supplemental Table S2. All
570 primers used are listed in Supplemental Table S3. For all fusion constructs, transcriptional and
571 translational fusions were verified by DNA sequencing. Plasmids were transformed into laboratory
572 strain Guy11 (Leung et al., 1988) using *Agrobacterium tumefaciens*–mediated transformation
573 (Khang et al., 2006). In several cases, two fluorescently labelled effectors were introduced by co-
574 transformation with separate plasmids (Sweigard et al., 1995). For each plasmid construct, 10
575 independent transformants were assayed for fluorescence intensity during host invasion and for
576 consistent localization patterns. Transformants with high fluorescence intensities were stored and
577 studied further (see Supplemental Table S1 online). For each construct cloned in *M. oryzae*, at
578 least two independent transformants showing identical sporulation, growth and infection
579 phenotypes to the wild type were selected and assayed together.

580 **Strategies for targeted deletion of Bas83 gene**

581 *Split-marker recombination method for Bas83 gene knockout via protoplast transformation*:
582 Targeted gene replacement mutation of the *M. oryzae Bas83* gene was attempted using the split
583 marker strategy as modified by Kershaw and Talbot (2009). Gene replacement was performed by
584 replacing the 606-bp *Bas83* locus with a hygromycin resistance selectable marker, encoding a 1.4-
585 kb hygromycin phosphotransferase (*HPH*) resistance cassette (Carroll et al., 1994). The two
586 overlapping segments of the *HPH* templates were PCR amplified using primers M13F with HY
587 and M13R with YG (Catlett et al., 2003) (see Supplemental Table S3 online) as described
588 previously (Kershaw and Talbot, 2009). One-kb DNA fragments upstream and downstream of the
589 *Bas83* open reading frame were generated using the primers Bas83LF-F and Bas83LFHY-R and
590 Bas83RFYG-F and Bas83RF-R amplified from genomic DNA of the Guy11 strain. A second-
591 round PCR reaction was performed to fuse the overlapping split hph marker templates with the
592 left and right flanking regions of the Bas83 locus. Wild-type *M. oryzae* strain Guy11 was then
593 transformed with the deletion cassettes (2 μg of each flank). Putative transformants were selected
594 in the presence of hygromycin B (200 μg/ml) and analyzed by PCR using the primers
595 Bas83:BASKOtest-F and Bas83:BASKOtest-R (Supplemental Table S3; Supplemental Figure
596 S5). This assay was repeated three times. Gene sequences on either side of *Bas83* were retrieved
597 from the NCBI database (https://www.ncbi.nlm.nih.gov/).

598 *Attempted Bas83 deletion via Agrobacterium-mediated transformation*: For gene
599 replacement transformation, cassettes were constructed by amplifying ~1.0 kb of 5′- and 3′-
600 flanking regions for each predicted coding sequence. The *HPH* gene (Carroll et al., 1994) was
601 cloned between the two flanking regions using a fusion PCR strategy. The three pieces together
602 were cloned first into the pJET1.6 vector (Invitrogen) for sequence analysis and later into binary
603 vector pGKO2 (Addgene: Plasmid #63617; Khang et al., 2005) using a restriction ligation strategy.
604 *M. oryzae* KU70 and KU80 spores were transformed using *A. tumefaciens* (Khang et al., 2005)
605 strains AGL1 and EHA105 (Hellens et al., 2000). After two rounds of selection in TB3 media
606 containing 200 μg/mL of hygromycin, 400 independent fungal transformants were analyzed for
607 gene replacement events by PCR amplification using the primers Bas83:BASKOtest-F and
608 Bas83:BASKOtest-R (Supplemental Figure S4). This assay was repeated three times.

609

610 **Staining with FM4-64, FM1-43, and Rhodamine Phalloidin, and treatment with**
611 **pharmacological inhibitors**
612 To examine membrane dynamics at the BIC, rice sheaths (cv. YT16) were inoculated with *M.*
613 *oryzae* transformants expressing fluorescently-labeled effectors ($2x10^4$ spores/ml in 0.25% gelatin
614 solution) and incubated for 20-26 hours at 25˚C for subsequent FM-dye treatment. Infected rice
615 sheaths were treated with FM4-64 or FM1-43 (4 mg/ml in water). An aqueous 17mM stock
616 solution of FM4-64 (Cat #13320, Invitrogen, Carlsbad, CA) and FM1-43 (Cat # T3163, Invitrogen,
617 Carlsbad, CA) were prepared and stored at -20˚C as described (45). *In planta*, inoculated leaf
618 sheaths, 24 h.p.i., were hand-trimmed into thin sections (3-7 layers of cells; 10 x 10 mm) and
619 incubated in a 10-mM aqueous working solution for 3–5 hours. Leaf sheaf sections were
620 subsequently transferred to ultrapure water and incubated for 20 min (25 ˚C) to remove excess
621 dyes for uniform membrane staining. For *in planta* experiments with Rhodamine Phalloidin (Cat#
622 R415, ThermoFisher Scientific), we prepared working solutions of 66 µM in 0.1% DMSO and
623 treated the inoculated tissue as described for FM dyes.
624 To examine the effects of endocytosis inhibitors on *in planta* effector uptake, inoculated
625 trimmed rice sheaths were incubated at 25˚C with Endosidin9 (ES9) (10µM), or Endosidin9-17
626 (ES9-17) (30µM), or Methyl-β-cyclodextrin (20 mM), or Chlorpromazine (10 µg/mL), or
627 Cantharidin (25 mM), or Fluazinam (20 mM), or Triclosan (20mM), or Wortmannin (20 nM), or
628 Concanamycin A (50 mM) (all from Sigma) solution for 1-5 hours. Negative controls were
629 performed with ultrapure water (Methyl-β-cyclodextrin, Chlorpromazine, and Fluazinam) or 0.1%
630 DMSO (ES9, ES9-17, Cantharidin, Filipin and Wortamanin) (see Table 1).

631 **Generation of transgenic rice plants**
632 Production of transgenic plants expressing the rice plant plasma membrane marker low-
633 temperature inducible protein 6B, LTi6B:GFP was previously described (Mentlak et al., 2012;
634 Giraldo et al., 2013). Transformants of rice cultivar Sasanishiki expressing LifeAct:eGFP were
635 generated in the laboratory of NJT. Expression plasmids for CME and CIE marker genes were
636 constructed by PCR amplifying the marker gene regions and fusing them to the N-terminus of
637 eGFP. The *CLC1* gene was amplified from genomic DNA of YT16 rice using the primers
638 KpnI_OsCLC1Prom1-F1 and XhoI_OsCLC1-R1 (See Supplemental Table S3). The PCR product
639 was digested with *Kpn*I and *Xho*I and integrated into pSH1.6EGFP (Plasmid #42323, Addgene).
640 The *Flot1* gene was amplified from genomic DNA from YT16 rice using the primers

641 HindIII_OsFlot1Prom1-F1 and Eco47III_OsFlot-R1. The PCR product was digested with *Hind*III
642 and *Eco*47III and integrated into pSH1.6EGFP. CLC1:eGFP was amplified from
643 pSH1.6_CLC1:eGFP using the primers CACC_OsCLC1-F1 and eGFPT2-R2, and cloned into
644 pENTR (pENTR™/D-TOPO™ Cloning Kit, ThermoFisher Scientific) following the
645 manufacturer's protocol. Flot1:eGFP was amplified form pSH1.6_Flot1:eGFP using the primers
646 CACC_OsFlot1-F1 and eGFPT2-R2, and cloned into pENTR following manufacturer's protocols.
647 The endocytosis marker:eGFP constructs were cloned into the *Agrobacterium* vector pIPKb001
648 (Himmelbach et al., 2007) using the Gateway LR Clonase II kit (Invitrogen) following the
649 manufacturer's protocol. All the fusion constructs had transcriptional and translational fusions
650 verified by DNA sequencing. Gene fusions for expressing the rice endocytosis markers
651 CLC1:eGFP (CME) and Flot1:eGFP (CIE) under their native promoters were introduced into
652 *Agrobacterium tumefaciens* EHA105 using the freeze-thaw method (Holsters et al., 1978). Mature
653 seed-derived callus from rice (*Oryza sativa L. Japonica*) cv. YT16 was used for *Agrobacterium*-
654 mediated transformation (Park et al., 2001). After inoculating with *A. tumefaciens*, callus was
655 transferred to regeneration medium for 4-10 weeks at 25˚C under a 16-h photoperiod. The
656 regenerated shoots were transferred to rooting medium for four more weeks, then established in
657 soil. Putative transformants of rice were selected on 100 µg/ml hygromycin, and expression
658 checked by qRT–PCR and epifluorescence microscopy. Thirty independent T1 transgenic lines
659 with CLC1:eGFP and 28 independent T1 lines with Flot1:eGFP were recovered. All lines were
660 assayed by microscopy for fluorescence pattern and for fluorescence intensity. All lines for each
661 construct showed the predicted fluorescence pattern. We chose lines with the highest levels of
662 fluorescence for assays.

663 **Silencing of rice genes**

664 In order to evaluate the role of plant endocytosis on disease development and effector uptake, we
665 performed VIGS using the Brome mosaic virus system developed by R.S. Nelson (Noble
666 Foundation, Ardmore, OK). We targeted *AP-2α*, *CHC1* (CME) and *Flot1* (CIE) mRNA in rice
667 plants (cultivar IR64) undergoing infection. The target rice sequences were cloned in the pC13/F3-
668 13m VIGS vector as described (Ding et al., 2006; Ding et al., 2007) and subsequently sequenced
669 to verify sequence accuracy. RNA transcripts were synthesized from the final VIGS vector. An
670 empty vector pC13/F3-13m was used as negative control. The final infectious transcripts of
671 pC13/F3-13m / AP-2α, pC13/F3-13m / CHC1, pC13/F3-13m /Flot1 and pC13/F3-13m (a control

672 virus without an insert) were inoculated with pC13/F1+2 in 7 to 10 days old IR64 rice plants
673 according to protocols described by Ding et al (2006). Knockdown of the target genes was
674 confirmed by qRT-PCR at 15 days post inoculation. At this point, rice plants showing satisfactory
675 reduction of the transcription levels were used in our standard conidial spray inoculation and leaf
676 sheath assays with fungal strains expressing fluorescently-labeled effectors.

677 **Statistics**

678 All experiments were performed with at least 3 biological replications, which are independent
679 experiments with fungal cultures directly growing out from frozen storage and different rice
680 plantings. Biological replications included at least two technical repeats (independent assays with
681 the same biological materials) for further confirming reproducibility of the data. In all cases,
682 technical and biological replications gave consistent results. Sample sizes, number of biological
683 replicates, and the statistical tests used in each experiment are specified in the figure legends. Data
684 were analyzed using an unpaired two-tailed Student's t-test. P=0.05 was considered non-
685 significant and exact values are shown where appropriate. All statistical analysis was performed
686 using R Statistical Software (version 4.1.2) and Prism9 (GraphPad). Dot plots were routinely used
687 to show individual data points and generated using Prism9 (GraphPad). Bar graphs show the
688 mean±s.e.m. (unless stated otherwise) and were generated using Prism9 (GraphPad). Analysis of
689 non-normal datasets are represented by box-and-whisker plots that show the 25th and 75th
690 percentiles, the median indicated by a horizontal line, and the minimum and maximum values
691 indicated by the ends of the whiskers.

692

693 **Accession Numbers**

694 Sequence data for genes of *M. oryzae* used in this article can be found in the GenBank/EMBL
695 database under the following accession numbers: BAS1, FJ807764.1/NC_017844; PWL1,
696 U36923.1; PWL2, U26313.1/NC_017853; Bas4, FJ807767.1/NC_017852.1; BAS83,
697 MGG_08506.6/NC_017851.1; BAS170, MGG_07348.6/NC_017850.1. Rice genes used are:
698 Clathrin Light Chain-1 (CLC1), LOC4337419; Flotilin 1 (Flot1), LOC4348926; Adaptor protein
699 complex-2α (AP-2α), LOC4331370; and Clathrin Heavy Chain-1 (CHC1 gene; LOC4349546.

700

701 **ACKNOWLEDGEMENTS**

We acknowledge and thank Rick Nelson (Noble Foundation, Ardmore, OK) for providing the VIGS vectors and hosting E.O.-G. in his laboratory to learn the VIGS assay. We thank the Talbot laboratory for assistance and hospitality during a working visit for E.O.-G at the University of Exeter. We thank Hiromasa Saitoh (Iwate Biotechnology Research Center, Kitakami, Iwate, Japan) and Ryohei Terauchi (Iwate Biotechnology Research Center, Kitakami, Iwate, and Kyoto University, Japan) for sharing transgenic rice expressing plant plasma membrane marker LTi6B:GFP. This project was supported by Agriculture and Food Research Initiative Competitive Grant no. #2017-67013-26525 from the USDA National Institute of Food and Agriculture Plant Biotic Interactions program. Additional support came from Louisiana State University Agricultural Center Hatch project #LAB94477 and from Louisiana Board of Regents grant #LEQSF(2022-24)-RD-A-01. This is Contribution no. 22-053-J from the Kansas Agricultural Experiment Station.

AUTHOR CONTRIBUTIONS

E.O.-G. and B.V. designed experiments and analyzed data: E.O.-G. performed most of the research. T.M.T., J.P. and S.P. produced and analyzed transgenic rice lines expressing the rice CLC1:eGFP and Flot1:eGFP fluorescent fusion protein genes. M.D., M.M.-U., C.R.H. and A.H.V. assisted with microscopy and Bas83 knockout experiments and general laboratory experiments; N.J.T. provided transgenic rice lines expressing LTi6B:GFP and LifeACT:GFP; E.O.-G., B.V. and N.J.T wrote and edited the article.

REFERENCES

Atkinson, H.A., Daniels, A., and Read, N.D. 2002. Live-cell imaging of endocytosis during conidial germination in the rice blast fungus, *Magnaporthe grisea*. Fungal Gen. Biol. 37:233-244.

Beck, M., Heard, W., Mbengue, M., and Robatzek, S. 2012. The INs and OUTs of pattern recognition receptors at the cell surface. Curr. Opin. Plant Biol. 15:367-374.

Bolte, S., Talbot, C., Boutte, Y., Catrice, O., Read, N.D., and Satiat-Jeunemaitre, B. 2004. FM-dyes as experimental probes for dissecting vesicle trafficking in living plant cells. Journal of Microscopy 214:159-173.

732 Bozkurt, T.O., Belhaj, K., Dagdas, Y.F., Chaparro-Garcia, A., Wu, C.-H., Cano, L.M., and
733 Kamoun, S. 2015. Rerouting of plant late endocytic trafficking toward a pathogen interface.
734 Traffic 16:204-226.
735 Bright, N.A., Lindsay, M.R., Stewart, A., and Luzio, J.P. 2001. The relationship between lumenal
736 and limiting membranes in swollen late endocytic compartments formed after wortmannin
737 treatment or sucrose accumulation. Traffic 2:631-642.
738 Carroll, A., Sweigard, J. A., and Valent, B. 1994. Improved vectors for selecting resistance to
739 hygromycin. 41:Article 5. https://newprairiepress.org/fgr/vol41/iss41/45/.
740 Catlett, N. L., Lee, B.-N., Yoder, O. C., and Turgeon, B. G. 2003. Split-marker recombination for
741 efficient targeted deletion of fungal genes. Fungal Genetics Newsletter 50:Article 4.
742 https://doi.org/10.4148/1941-4765.1150.
743 Chaparro-Garcia, A., Schwizer, S., Sklenar, J., Yoshida, K., Petre, B., Bos, J.I.B., Schornack, S.,
744 Jones, A.M.E., Bozkurt, T.O., and Kamoun, S. 2015. *Phytophthora infestans* RXLR-WY
745 effector AVR3a associates with dynamin-related protein 2 required for endocytosis of the
746 plant pattern recognition receptor FLS2. PLoS ONE 10:e0137071.
747 Chen, X., Irani, N.G., and Friml, J. 2011. Clathrin-mediated endocytosis: the gateway into plant
748 cells. Curr. Opin. Plant Biol. 14:674-682.
749 Collemare, J., Pianfetti, M., Houlle, A.E., Morin, D., Camborde, L., Gagey, M.J., Barbisan, C.,
750 Fudal, I., Lebrun, M.H., and Böhnert, H.U. 2008. *Magnaporthe grisea* avirulence gene *ACE1*
751 belongs to an infection-specific gene cluster involved in secondary metabolism. New Phytol.
752 179:196-208.
753 Dagdas, Y.F., Pandey, P., Tumtas, Y., Sanguankiattichai, N., Belhaj, K., Duggan, C., Leary, A.Y.,
754 Segretin, M.E., Contreras, M.P., Savage, Z., Khandare, V.S., Kamoun, S., and Bozkurt, T.O.
755 2018. Host autophagy machinery is diverted to the pathogen interface to mediate focal
756 defense responses against the Irish potato famine pathogen. eLife 7:e37476.
757 Dejonghe, W., and Russinova, E. 2017. Plant chemical genetics: From phenotype-based screens
758 to synthetic biology. Plant Physiology 174:5-20.
759 Dejonghe, W., Kuenen, S., Mylle, E., Vasileva, M., Keech, O., Viotti, C., Swerts, J., Fendrych,
760 M., Ortiz-Morea, F.A., Mishev, K., Delang, S., Scholl, S., Zarza, X., Heilmann, M., Kourelis,
761 J., Kasprowicz, J., Nguyen, L.S.L., Drozdzecki, A., Van Houtte, I., Szatmári, A.-M., Majda,
762 M., Baisa, G., Bednarek, S.Y., Robert, S., Audenaert, D., Testerink, C., Munnik, T., Van

763 Damme, D., Heilmann, I., Schumacher, K., Winne, J., Friml, J., Verstreken, P., and
764 Russinova, E. 2016. Mitochondrial uncouplers inhibit clathrin-mediated endocytosis largely
765 through cytoplasmic acidification. Nat. Comm. 7:11710.
766 Dejonghe, W., Sharma, I., Denoo, B. De Munck, S., Lu, Q., Mishev, K., Bulut, H., Mylle, E., De
767 Rycke, R., Vasileva, M., Savatin, D.V., Nerinckx, W., Staes, A., Drozdzecki, A., Audenaert,
768 D., Yperman, K., Madder, A., Friml, J,, Van Damme, D., Gevaert, K., Haucke, V., Savvides,
769 S.N., Winne, J., Russinova, E. 2019. Disruption of endocytosis through chemical inhibition
770 of clathrin heavy chain function. Nat. Chem. Biol. 15, 641–649.
771 Di Rubbo, S., Irani, N. G., Kim, S. Y., Xu, Z.-Y., Gadeyne, A., Dejonghe, W., Vanhoutte, I.,
772 Persiau, G., Eeckhout, D., Simon, S., Song, K., Kleine-Vehn, J., Friml, J., De Jaeger, G., Van
773 Damme, D., Hwang, I., and Russinova, E. 2013. The Clathrin Adaptor Complex AP-2
774 mediates endocytosis of BRASSINOSTEROID INSENSITIVE1 in *Arabidopsis*. Plant Cell
775 25:2986-2997.
776 Ding, X.S., Rao, C.S., and Nelson, R.S. 2007. Analysis of gene function in rice through virus-
777 induced gene silencing. Methods in molecular biology (Clifton, N.J.) 354:145-160.
778 Ding, X.S., Schneider, W.L., Chaluvadi, S.R., Mian, M.A.R., and Nelson, R.S. 2006.
779 Characterization of a Brome mosaic virus strain and its use as a vector for gene silencing in
780 monocotyledonous hosts. Mol. Plant-Microbe Interact. 19:1229-1239.
781 Dodds, P.N., and Rathjen, J.P. 2010. Plant immunity: towards an integrated view of plant-pathogen
782 interactions. Nat. Rev. Genet. 11:539-548.
783 Dutta, D. and Donaldson, J.G. 2012. Search for inhibitors of endocytosis. Cellular Logistics 2:203-
784 208.
785 Elsworth, B., Matthews, K., Nie, C.Q., Kalanon, M., Charnaud, S.C., Sanders, P.R., Chisholm,
786 S.A., Counihan, N.A., Shaw, P.J., Pino, P., Chan, J.A., Azevedo, M.F., Rogerson, S.J.,
787 Beeson, J.G., Crabb, B.S., Gilson, P.R., and de Koning-Ward, T.F. 2014. PTEX is an
788 essential nexus for protein export in malaria parasites. Nature 511:587-+.
789 Ewers, H., and Helenius, A. 2011. Lipid-mediated endocytosis. Cold Spring Harbor Perspectives
790 in Biology 3:10.1101/cshperspect.a004721.
791 Fan, L., Li, R., Pan, J., Ding, Z., and Lin, J. 2015. Endocytosis and its regulation in plants. Trends
792 in Plant Science 20:388-397.

793 Fawke, S., Doumane, M., and Schornack, S. 2015. Oomycete interactions with plants: infection
794 strategies and resistance principles. Microbiology and Molecular Biology Reviews 79:263-
795 280.
796 Fudal, I., Collemare, J., Böhnert, H.U., Melayah, D., and Lebrun, M.-H. 2007. Expression of
797 *Magnaporthe grisea* avirulence gene *ACE1* is connected to the initiation of appressorium-
798 mediated penetration. Eukaryotic Cell 6:546-554.
799 Giraldo, M.C., and Valent, B. 2013. Filamentous plant pathogen effectors in action. Nat. Rev.
800 Microbiol. 11:800-814.
801 Giraldo, M.C., Dagdas, Y.F., Gupta, Y.K., Mentlak, T.A., Yi, M., Martinez-Rocha, A.L., Saitoh,
802 H., Terauchi, R., Talbot, N.J., and Valent, B. 2013. Two distinct secretion systems facilitate
803 tissue invasion by the rice blast fungus *Magnaporthe oryzae*. Nat. Comm. 4:1996.
804 Gladieux, P., Condon, B., Ravel, S., Soanes, D., Maciel, J.L.N., Nhani, A., Chen, L., Terauchi, R.,
805 Lebrun, M.-H., Tharreau, D., Mitchell, T., Pedley, K.F., Valent, B., Talbot, N.J., Farman,
806 M., and Fournier, E. 2018. Gene flow between divergent cereal- and grass-specific lineages
807 of the rice blast fungus *Magnaporthe oryzae*. mBio 9:e01219-01217.
808 Grassart, A., Cheng, A.T., Hong, S.H., Zhang, F., Zenzer, N., Feng, Y., Briner, D.M., Davis, G.D.,
809 Malkov, D., and Drubin, D.G. 2014. Actin and dynamin2 dynamics and interplay during
810 clathrin-mediated endocytosis. Journal of Cell Biology 205:721-735.
811 Harder, D.E., and Mendgen, K. 1982. Filipin-sterol complexes in bean rust- and oat crown rust-
812 fungal/plant interactions: Freeze-etch electron microscopy. Protoplasma 112:46-54.
813 Hellens, R., Mullineaux, P., and Klee, H. 2000. Technical Focus: a guide to *Agrobacterium* binary
814 Ti vectors. Trends Plant Sci. 5:446-451.
815 Hicks, G.R., and Raikhel, N.V. 2010. Advances in dissecting endomembrane trafficking with
816 small molecules. Curr. Opin. Plant Biol. 13:706-713.
817 Himmelbach, A., Zierold, U., Hensel, G., Riechen, J., Douchkov, D., Schweizer, P., and Kumlehn,
818 J. 2007. A set of modular binary vectors for transformation of cereals. Plant Physiology
819 145:1192-1200.
820 Holsters, M., de Waele, D., Depicker, A., Messens, E., van Montagu, M., and Schell, J. 1978.
821 Transfection and transformation of *Agrobacterium tumefaciens*. Molecular and General
822 Genetics 163:181-187.

823 Howard, R.J., and Valent, B. 1996. Breaking and Entering: Host penetration by the fungal rice
824 blast pathogen *Magnaporthe grisea*. Annu. Rev. Microbiol. 50:491-512.
825 Johnson, A., Gnyliukh, N., Kaufmann, W.A., Narasimhan, M., Vert, G., Bednarek, S.Y., and
826 Friml, J. 2020. Experimental toolbox for quantitative evaluation of clathrin-mediated
827 endocytosis in the plant model *Arabidopsis*. Journal of Cell Science 133:jcs248062.
828 Jones, K., Zhu, J., Jenkinson, C.B., Kim, D.W., Pfeifer, M.A., and Khang, C.H. 2021. Disruption
829 of the interfacial membrane leads to *Magnaporthe oryzae* effector re-location and lifestyle
830 switch during rice blast disease. Frontiers in Cell and Developmental Biology
831 9:10.3389/fcell.2021.681734.
832 Kaksonen, M., and Roux, A. 2018. Mechanisms of clathrin-mediated endocytosis. Nat. Rev. Mol.
833 Cell Biol. 19:313-326.
834 Kale, S.D., Gu, B., Capelluto, D.G.S., Dou, D., Feldman, E., Rumore, A., Arredondo, F.D.,
835 Hanlon, R., Fudal, I., Rouxel, T., Lawrence, C.B., Shan, W., and Tyler, B.M. 2010. External
836 lipid PI3P mediates entry of eukaryotic pathogen effectors into plant and animal host cells.
837 Cell 142:284-295.
838 Kankanala, P., Czymmek, K., and Valent, B. 2007. Roles for rice membrane dynamics and
839 plasmodesmata during biotrophic invasion by the blast fungus. Plant Cell 19:706-724.
840 Kato, H. 1974. Epidemiology of rice blast disease. Review of Plant Protection Research 7:1-20.
841 Kershaw, M. J., and Talbot, N. J. 2009. Genome-wide functional analysis reveals that infection-
842 associated fungal autophagy is necessary for rice blast disease. Proceedings of the National
843 Academy of Sciences U.S.A. 106:15967-15972.
844 Khang, C.H., Park, S., Rho, H., Lee, Y., and Kang, S. 2006. *Agrobacterium tumefaciens*-mediated
845 transformation and mutagenesis of filamentous fungi *Magnaporthe grisea* and *Fusarium*
846 *oxysporum*. in: Agrobacterium Protocols, K. Wang, ed. Humana Press, Totowa.
847 Khang, C.H., Berruyer, R., Giraldo, M.C., Kankanala, P., Park, S.-Y., Czymmek, K., Kang, S.,
848 and Valent, B. 2010. Translocation of *Magnaporthe oryzae* effectors into rice cells and their
849 subsequent cell-to-cell movement. Plant Cell 22:1388-1403.
850 Kleemann, J., Rincon-Rivera, L.J., Takahara, H., Neumann, U., Ver Loren van Themaat, E., van
851 der Does, H.C., Hacquard, S., Stüber, K., Will, I., Schmalenbach, W., Schmelzer, E., and
852 O'Connell, R.J. 2012. Sequential delivery of host-induced virulence effectors by appressoria

853 and intracellular hyphae of the phytopathogen *Colletotrichum higginsianum*. PLoS Path.
854 8:e1002643.
855 Konopka, C.A., Backues, S.K., and Bednarek, S.Y. 2008. Dynamics of Arabidopsis Dynamin-
856 Related Protein 1C and a Clathrin Light Chain at the plasma membrane. Plant Cell 20:1363-
857 1380.
858 Larson, E. R., Van Zelm, E., Roux, C., Marion-Poll, A., and Blatt, M. R. 2017. Clathrin heavy
859 chain subunits coordinate endo- and exocytic traffic and affect stomatal movement. Plant
860 Physiol. 175:708-720.
861 Leung, H., Borromeo, E.S., Bernardo, M.A., and Notteghem, J.L. 1988. Genetic analysis of
862 virulence in the rice blast fungus *Magnaporthe grisea*. Phytopathology 78:1227-1233.
863 Li, R., Liu, P., Wan, Y., Chen, T., Wang, Q., Mettbach, U., Baluška, F., Samaj, J., Fang, X., Lucas,
864 W.J., and Lin, J. 2012. A membrane microdomain-associated protein, *Arabidopsis* Flot1, is
865 involved in a clathrin-independent endocytic pathway and is required for seedling
866 development. Plant Cell 24 2105-2122
867 Lo Presti, L., and Kahmann, R. 2017. How filamentous plant pathogen effectors are translocated
868 to host cells. Curr. Opin. Plant Biol. 38:19-24.
869 Lo Presti, L., Zechmann, B., Kumlehn, J., Liang, L., Lanver, D., Tanaka, S., Bock, R., and
870 Kahmann, R. 2017. An assay for entry of secreted fungal effectors into plant cells. New
871 Phytol. 213:956-964.
872 Lo Presti, L., Lanver, D., Schweizer, G., Tanaka, S., Liang, L., Tollot, M., Zuccaro, A., Reissmann,
873 S., and Kahmann, R. 2015. Fungal effectors and plant susceptibility. Annual Review of Plant
874 Biology 66:513-545.
875 Ludwig, N., Reissmann, S., Schipper, K., Gonzalez, C., Assmann, D., Glatter, T., Moretti, M., Ma,
876 L.-S., Rexer, K.-H., Snetselaar, K., and Kahmann, R. 2021. A cell surface-exposed protein
877 complex with an essential virulence function in *Ustilago maydis*. Nature Microbiology
878 6:722-730.
879 Manning, V.A., and Ciuffetti, L.M. 2005. Localization of Ptr ToxA produced by *Pyrenophora*
880 *tritici-repentis* reveals protein import into wheat mesophyll cells. Plant Cell 17:3203-3212.
881 Maranda, B., Brown, D., Bourgoin, S., Casanova, J.E., Vinay, P., Ausiello, D.A., and Marshansky,
882 V. 2001. Intra-endosomal pH-sensitive recruitment of the Arf-nucleotide exchange factor

883 ARNO and Arf6 from cytoplasm to proximal tubule endosomes. Journal of Biological
884 Chemistry 276:18540-18550.
885 Mbengue, M., Bourdais, G., Gervasi, F., Beck, M., Zhou, J., Spallek, T., Bartels, S., Boller, T.,
886 Ueda, T., Kuhn, H., and Robatzek, S. 2016. Clathrin-dependent endocytosis is required for
887 immunity mediated by pattern recognition receptor kinases. Proceedings of the National
888 Academy of Sciences 113:11034-11039.
889 Mentlak, T.A., Kombrink, A., Shinya, T., Ryder, L.S., Otomo, I., Saitoh, H., Terauchi, R.,
890 Nishizawa, Y., Shibuya, N., Thomma, B.P., and Talbot, N.J. 2012. Effector-mediated
891 suppression of chitin-triggered immunity by *Magnaporthe oryzae* is necessary for rice blast
892 disease. Plant Cell 24:322-335.
893 Mochizuki, S., Minami, E., and Nishizawa, Y. 2015. Live-cell imaging of rice cytological changes
894 reveals the importance of host vacuole maintenance for biotrophic invasion by blast fungus,
895 *Magnaporthe oryzae*. MicrobiologyOpen 4:952-966.
896 Mosquera, G., Giraldo, M.C., Khang, C.H., Coughlan, S., and Valent, B. 2009. Interaction
897 transcriptome analysis identifies *Magnaporthe oryzae* BAS1-4 as biotrophy-associated
898 secreted proteins in rice blast disease. Plant Cell 21:1273-1290.
899 Narasimhan, M., Johnson, A., Prizak, R., Kaufmann, W.A., Tan, S., Casillas-Pérez, B., and Friml,
900 J. 2020. Evolutionarily unique mechanistic framework of clathrin-mediated endocytosis in
901 plants. eLife 9:e52067.
902 Nishimura, T., Mochizuki, S., Ishii-Minami, N., Fujisawa, Y., Kawahara, Y., Yoshida, Y., Okada,
903 K., Ando, S., Matsumura, H., Terauchi, R., Minami, E., and Nishizawa, Y. 2016.
904 *Magnaporthe oryzae* glycine-rich secretion protein, Rbf1 critically participates in
905 pathogenicity through the focal formation of the biotrophic interfacial complex. PLoS Path.
906 12:e1005921.
907 Nishizawa, Y., Mochizuki, S., Yokotani, N., Nishimura, T., and Minami, E. 2016. Molecular and
908 cellular analysis of the biotrophic interaction between rice and *Magnaporthe oryzae* –
909 Exploring situations in which the blast fungus controls the infection. Physiol. Mol. Plant
910 Pathol. 95:70-76.
911 O'Connell, R.J., and Panstruga, R. 2006. Tête à tête inside a plant cell: establishing compatibility
912 between plants and biotrophic fungi and oomycetes. New Phytol. 171:699-718.

913 Oliveira-Garcia, E., and Valent, B. (2021). Characterizing the secretion systems of *Magnaporthe*
914 *oryzae* . In: Jacob, S. (eds) *Magnaporthe oryzae*. Methods in Molecular Biology, vol 2356.
915 Humana, New York, NY. https://doi.org/10.1007/978-1-0716-1613-0_5
916 Otto, G.P., and Nichols, B.J. 2011. The roles of flotillin microdomains – endocytosis and beyond.
917 Journal of Cell Science 124:3933-3940.
918 Park, S.H., Park, J., and Smith, R.H. 2001. Herbicide and insect resistant elite transgenic rice.
919 Journal of Plant Physiology 158:1221-1226.
920 Petre, B., and Kamoun, S. 2014. How do filamentous pathogens deliver effector proteins into plant
921 cells? PLoS. Biol. 12:e1001801.
922 Petre, B., Contreras, M.P., Bozkurt, T.O., Schattat, M.H., Sklenar, J., Schornack, S., Abd-El-
923 Haliem, A., Castells-Graells, R., Lozano-Durán, R., Dagdas, Y.F., Menke, F.L.H., Jones,
924 A.M.E., Vossen, J.H., Robatzek, S., Kamoun, S., and Win, J. 2021. Host-interactor screens
925 of *Phytophthora infestans* RXLR proteins reveal vesicle trafficking as a major effector-
926 targeted process. Plant Cell 33:1447-1471.
927 Postma, J., Liebrand, T.W.H., Bi, G., Evrard, A., Bye, R.R., Mbengue, M., Kuhn, H., Joosten,
928 M.H.A.J., and Robatzek, S. 2016. Avr4 promotes Cf-4 receptor-like protein association with
929 the BAK1/SERK3 receptor-like kinase to initiate receptor endocytosis and plant immunity.
930 New Phytol. 210:627-642.
931 Qi, X., Pleskot, R., Irani, N.G., and Van Damme, D. 2018. Meeting report – Cellular gateways:
932 expanding the role of endocytosis in plant development. Journal of Cell Science
933 131:jcs222604.
934 Reynolds, G.D., Wang, C., Pan, J., and Bednarek, S.Y. 2018. Inroads into internalization: Five
935 years of endocytic exploration. Plant Physiology 176:208-218.
936 Robinson, D.G., Jiang, L.W., and Schumacher, K. 2008. The endosomal system of plants: Charting
937 new and familiar territories. Plant Physiology 147:1482-1492.
938 Rodal, S.K., Skretting, G., Garred, O., Vilhardt, F., van Deurs, B., and Sandvig, K. 1999.
939 Extraction of cholesterol with methyl-beta-cyclodextrin perturbs formation of clathrin-
940 coated endocytic vesicles. Molecular Biology of the Cell 10:961-974.
941 Ruan, H., Li, J., Wang, T., Ren, H. Secretory vesicles targeted to plasma membrane during pollen
942 germination and tube growth. 2021. Front. Cell Dev. Biol. 8:615447.

943 Sachse, M., Urbe, S., Oorschot, V., Strous, G.J., and Klumperman, J. 2002. Bilayered clathrin
944 coats on endosomal vacuoles are involved in protein sorting toward lysosomes Molecular
945 Biology of the Cell 13:1313-1328
946 Sakulkoo, W., Oses-Ruiz, M., Garcia, E.O., Soanes, D.M., Littlejohn, G.R., Hacker, C., Correia,
947 A., Valent, B., and Talbot, N.J. 2018. A single fungal MAP kinase controls plant cell-to-cell
948 invasion by the rice blast fungus. Science 359:1399-1403.
949 Schneider, C.A., Rasband, W.S., Eliceiri, K.W. 2012. "NIH Image to ImageJ: 25 years of image
950 analysis". Nature Methods 9, 671-675.
951 Schuh, M. (2011). An actin-dependent mechanism for long-range vesicle transport. Nature Cell
952 Biology, 13(12), 1431-1436.
953 Serrano, M., Robatzek, S., Torres, M., Kombrink, E., Somssich, I.E., Robinson, M., and Schulze-
954 Lefert, P. 2007. Chemical interference of pathogen-associated molecular pattern-triggered
955 immune responses in Arabidopsis reveals a potential role for fatty-acid synthase type II
956 complexderived lipid signals. Journal of Biological Chemistry 282:6803-6811.
957 Spallek, T., Beck, M., Ben Khaled, S., Salomon, S., Bourdais, G., Schellmann, S., and Robatzek,
958 S. 2013. ESCRT-I mediates FLS2 endosomal sorting and plant immunity. PLoS Genetics
959 9:e1004035.
960 Stark-Urnau, M., and Mendgen, K. 1995. Sequential deposition of plant glycoproteins and
961 polysaccharides at the host-parasite interface of *Uromyces vignae* and *Vigna sinensis*:
962 Evidence for endocytosis and secretion. Protoplasma 186:1-11.
963 Sweigard, J. A., Carroll, A. M., Kang, S., Farrall, L., Chumley, F. G., and Valent, B. 1995.
964 Identification, cloning, and characterization of *PWL2*, a gene for host species specificity in
965 the rice blast fungus. Plant Cell 7:1221-1233.
966 Trusch, F., Loebach, L., Wawra, S., Durward, E., Wuensch, A., Iberahim, N.A., de Bruijn, I.,
967 MacKenzie, K., Willems, A., Toloczko, A., Diéguez-Uribeondo, J., Rasmussen, T.,
968 Schrader, T., Bayer, P., Secombes, C.J., and van West, P. 2018. Cell entry of a host-targeting
969 protein of oomycetes requires gp96. Nat. Comm. 9:2347.
970 Valent, B., and Chumley, F.G. 1991. Molecular genetic analysis of the rice blast fungus,
971 *Magnaporthe grisea*. Annu. Rev. Phytopathol. 29:443-467.
972 Valent, B., Singh, P.K., He, X., Farman, M., Tosa, Y., and Braun, H.J. 2020. Blast diseases:
973 Evolution and challenges of a staple food crop fungal pathogen. Pages 267-292 in: Emerging

974 Plant Diseases and Global Food Security, J.B. Ristaino and A. Records, eds. American
975 Phytopathological Society Press, St. Paul, MN.
976 Van den Ackerveken, G. 2017. Seeing is believing: imaging the delivery of pathogen effectors
977 during plant infection. New Phytol. 216:8-10.
978 Wang, L.H., Rothberg, K.G., and Anderson, R.G. 1993. Misassembly of clathrin lattices on
979 endosomes reveals a regulatory switch for coated pit formation Journal of Cell Biology
980 123:1107-1117.
981 Wang, S., Boevink, P.C., Welsh, L., Zhang, R., Whisson, S.C., and Birch, P.R.J. 2017. Delivery
982 of cytoplasmic and apoplastic effectors from *Phytophthora infestans* haustoria by distinct
983 secretion pathways. New Phytol. 216:205-215.
984 Wawra, S., Trusch, F., Matena, A., Apostolakis, K., Linne, U., Zhukov, I., Stanek, J., Koźmiński,
985 W., Davidson, I., Secombes, C.J., Bayer, P., and van West, P. 2017. The RxLR motif of the
986 host targeting effector AVR3a of *Phytophthora infestans* is cleaved before secretion. Plant
987 Cell 29:1184-1195.
988 Xu, J.-R., Staiger, C.J., and Hamer, J.E. 1998. Inactivation of the mitogen-activated protein
989 kinase Mps1 from the rice blast fungus prevents penetration of host cells but allows
990 activation of plant defense responses. Proceedings of the National Academy of Sciences
991 U.S.A. 95:12713-12718
992 Yan, X., Tang, B., Ryder, L. S., MacLean, D., Were, V. M., Eseola, A. B., Cruz-Mireles, N.,
993 Foster, A. J., Osés-Ruiz, M. and Talbot, N. J. 2022. The transcriptional landscape of plant
994 infection by the rice blast fungus *Magnaporthe oryzae* reveals distinct families of
995 temporally co-regulated and structurally conserved effectors. bioRxiv:
996 2022.2007.2018.500532.

997 **Table 1. Chemical inhibitors of endocytosis**

Chemical	Target	Mode of action	Comments	References
Filipin	CIE*	Binds to sterols in the membrane.	Toxic at higher concentrations; some impact on CME.	Rodal et al., 1999; Dutta and Donaldson, 2012
Methyl-β-cyclodextrin	CIE	Deplete cellular membranes of sterols by increasing the water solubility of the sterol.	caveolae-dependent endocytosis; some impact on CME.	Rodal et al., 1999; Dutta and Donaldson, 2012
Chlorpromazine	CME**	Translocate clathrin and AP2 from the cell surface to intracellular endosomes.	Also inhibits CIE in some cells.	Wang et al., 1993; Dutta and Donaldson, 2012
Cantharidin	CME	Inhibits PP2A (protein phosphatase 2A)	Affects flg22-mediated FLS2 endocytosis by targeting signaling.	Serrano et al., 2007
Triclosan	CME	Inhibits PP2A (protein phosphatase 2A)	Affects flg22-mediated FLS2 endocytosis by targeting signaling.	Serrano et al., 2007
Wortmannin	nd***	Inhibits PI3Ks, blocks late trafficking to the vacuole, multivesicular bodies and endocytosis.	Late endosomes lose clathrin; Potential CME association.	Bright et al., 2001; Sachse et al., 2002; Robinson et al., 2008
Endosidin9	CME	Inhibits function of Clathrin Heavy Chain; has proton translocator activity	CHC inhibition in *Arabidopsis and Drosophila; causes cytoplasmic acidification*	Dejonghe, et al., 2019; Dejonghe, et al., 2016
Endosidin9-17	CME	Inhibits function of Clathrin Heavy Chain (CHC)	Inhibitor of CHC function in *Arabidopsis* and human cells. More specific version of ES9 lacking cytoplasmic acidification activity.	Dejonghe, et al., 2019
Concanamycin A	nd	Targets V-type ATPase and blocks trafficking at trans-Golgi network, endosome acidification.	Induces acidification crucial for endocytic pathways.	Maranda et al., 2001; Robinson et al., 2008

998 *CIE: clathrin-independent endocytosis; **CME: clathrin-mediated endocytosis; ***nd: not determined.

999

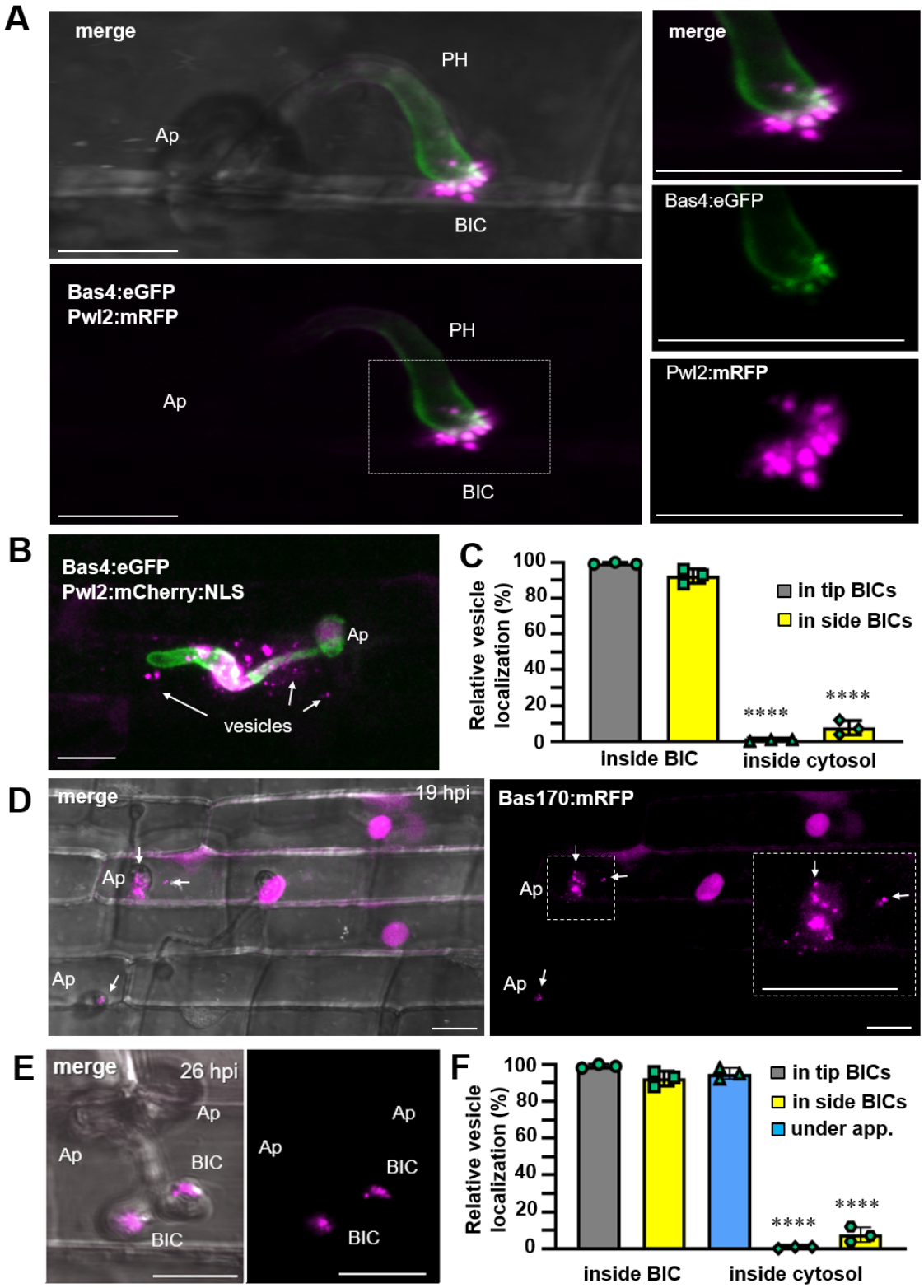
A
merge
PH
Ap
BIC
merge
Bas4:eGFP
Bas4:eGFP
Pwl2:mRFP
PH
Ap
BIC
Pwl2:mRFP
B
Bas4:eGFP
Pwl2:mCherry:NLS
Ap
vesicles
C
Relative vesicle localization (%)
100
80
60
40
20
0
in tip BICs
in side BICs
****
****
inside BIC
inside cytosol
D
merge
19 hpi
Ap
Ap
Bas170:mRFP
Ap
Ap
E
merge
26 hpi
Ap
Ap
BIC
BIC
Ap
Ap
BIC
BIC
F
Relative vesicle localization (%)
100
80
60
40
20
0
in tip BICs
in side BICs
under app.
****
****
inside BIC
inside cytosol

1000

1001 **Figure 1**. **BIC vesicular organization and effector vesicles in the rice cell cytoplasm**. **A.**
1002 Cytoplasmic effector-labeled vesicles in a BIC at the tip of a primary hypha (PH) of strain KV217
1003 expressing Pwl2:mRFP and Bas4:eGFP at 17 hpi. The appressorium (Ap) and the first half of the
1004 PH are out of focus. Merged mRFP (magenta) and eGFP (green), eGFP and mRFP inset channels
1005 (right) show the base layer of apoplastic effector Bas4:eGFP and the outer layer of cytoplasmic
1006 effector Pwl2:mRFP. Occurrence of effector vesicles is independent of the cytoplasmic effector or
1007 fluorescent protein used (Supplemental Figure S1). **B.** A side-BIC occurring above a first bulbous
1008 IH cell of strain KV168 expressing Pwl2:mCherry:NLS and Bas4:eGFP at 24 hpi. Effector vesicles
1009 are visible in the host cytoplasm at a distance from the BIC (arrows). The Bas4:eGFP control
1010 shows that the EIHM surrounding the IH remains intact. See Supplemental Figure S2 for a view
1011 of the entire invaded cell showing host translocation of nuclear targeted Pwl2:mCherry:NLS. **C.**
1012 Quantification of the relative localization of cytoplasmic effector vesicles, assessed using strain
1013 KV217 from panel A. 98 vesicles carrying Pwl2:mRFP counted for each BIC developmental stage.
1014 Bar charts are based on means of all data from three biological reps (data points show the means
1015 of the individual reps); error bars indicate standard deviation. ****P<0.0001. **D.** Bas170:mRFP,
1016 here expressed by *M. oryzae* strain KV224, shows rapid accumulation in vesicles under appressoria
1017 and in plant nuclei even before a primary hypha is visible. On the right, the enlarged inset
1018 highlights vesicles near the penetration site (arrows). Left image shows merged bright field and
1019 mRFP fluorescence and right image shows mRFP fluorescence alone. **E.** Bas170:mRFP also
1020 localizes to BICs, shown here in two side-BICs resulting from adjacent appressoria penetrating the
1021 same rice cell. Experimental details same as in D. **F.** Quantification of the relative localizations of
1022 Bas170:mRFP effector vesicles, assessed using strain KV224 (D and E). 100 vesicles carrying
1023 Bas170:mRFP counted for each BIC stage and cytoplasm under appressoria (app.). Bar charts
1024 same as described in C. All images are projections of confocal optical sections. Bars = 10 µm.

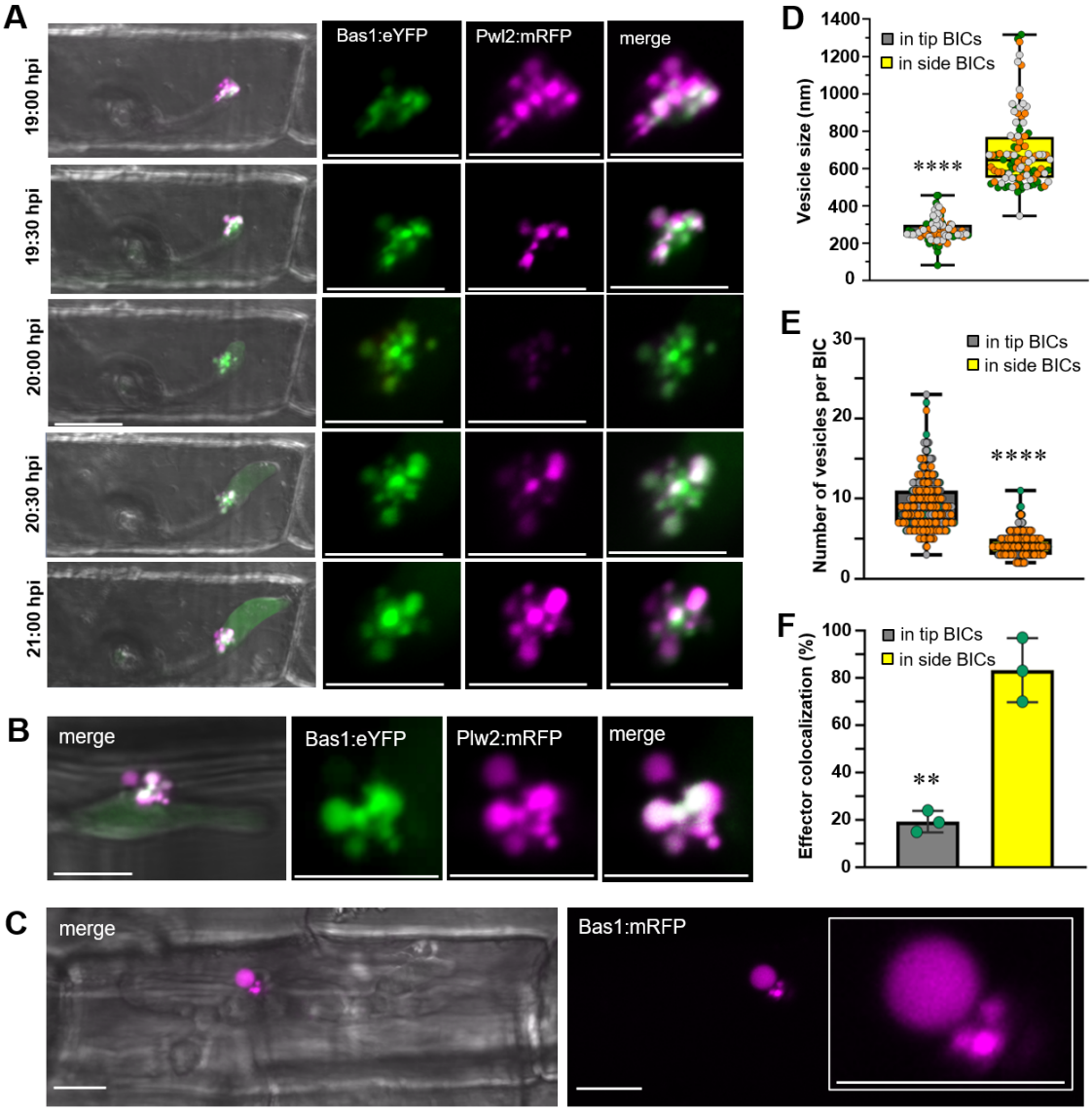

Figure 2. Dynamics of BICs and effector vesicles during differentiation of primary hyphae to first bulbous invasive hyphae. A. Two cytoplasmic effectors, Pwl2:mRFP and Bas1:eYFP (Strain KV211) were observed as a tip-BIC (top panel) becomes a side-BIC (bottom panel), imaged every 30 min from 19 to 21 hpi. Images (left to right) are merged bright field, eYFP (green) and mRFP (magneta) fluorescence at 5 time points; then enlarged views of eYFP alone, mRFP alone and merged eYFP and mRFP at same time points. Fluorescent BICs are shown as projections of confocal optical sections. Bars = 10 µm. **B.** Cytoplasmic effectors Pwl2:mRFP and Bas1:eYFP (Strain KV211) co-localize in larger vesicles in a side-BIC at 24 hpi. **C.** A rare extremely large effector vesicle (diameter 3.9 µm) in a late stage side-BIC formed by strain KV170 expressing Bas1:mRFP at 30 hpi. **D,E.** Box and whisker plots with individual data points comparing vesicle sizes (D) and number of vesicles (E) in tip- and side-BICs formed by strain KV211; data points of

1037 different colors represent different biological replicates. **F.** Bar chart showing quantification of
1038 Bas1:eYFP and Pwl2:mRFP colocalization (KV211) in vesicles in tip- and side-BICs. Bar charts
1039 are based on means of all data from three biological replicates (data points show the means of the
1040 individual reps); error bars indicate standard deviation. **P=0.0015; ****P<0.0001. 112 vesicles
1041 measured for tip- and side-BICs in D. 100 BICs observed per replicate in E-F.

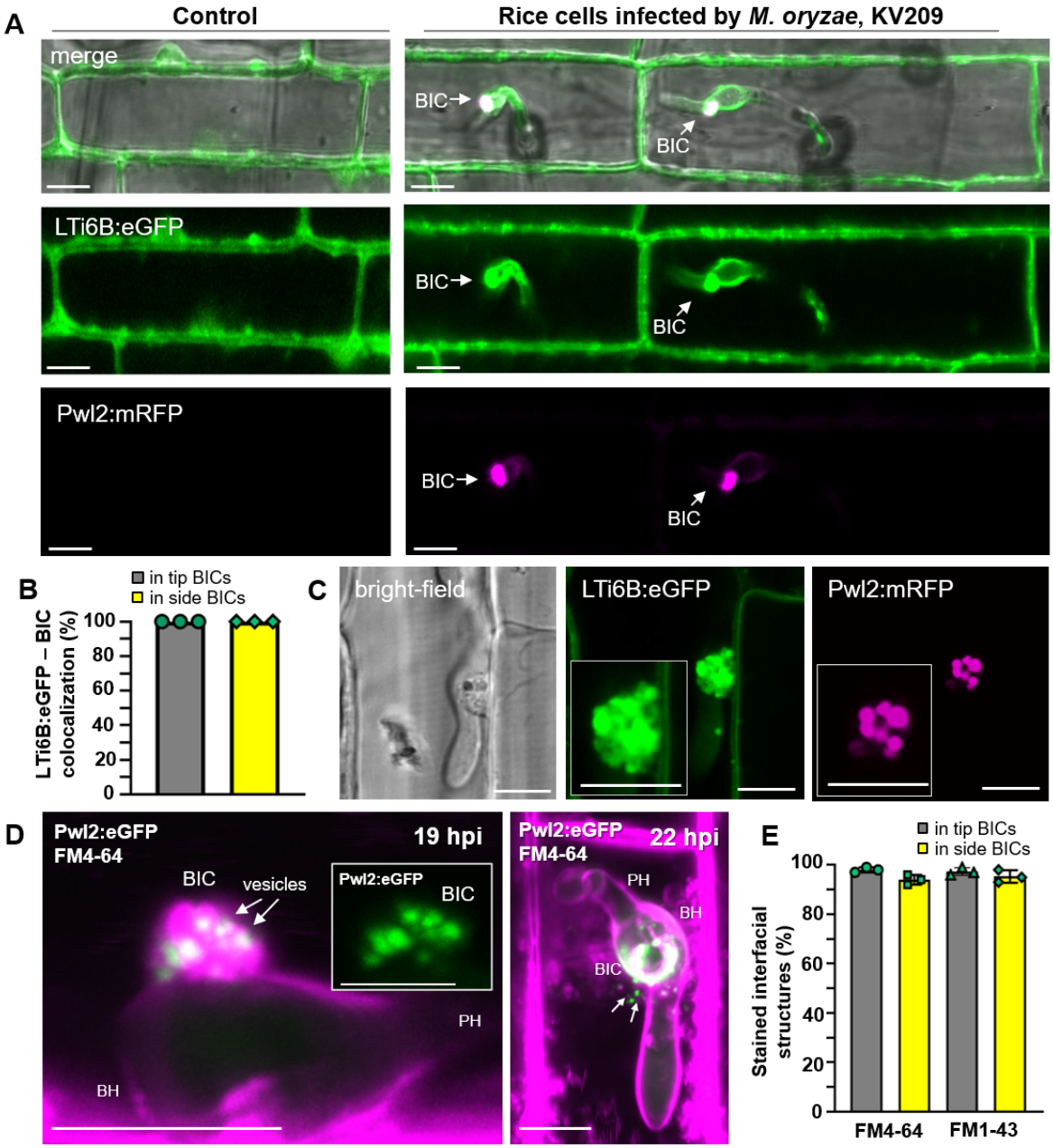

Figure 3. Effector vesicles are derived from plant plasma membrane. A. Rice expressing plasma membrane marker LTi6B:eGFP in non-infected cells (left column) and in cells infected by strain KV209 expressing Pwl2:mRFP (right column). Colocalization in a tip-BIC (left) and a side-BIC (right) confirms BICs as plant plasma membrane-rich structures. **B.** Quantification of the colocalization of LTi6B:eGFP with BICs. Bar charts are based on means of all data from three biological replicates (data points show the means of the individual reps); three times 90 infection sites observed. **C.** Localization assays of LTi6B:eGFP relative to Pwl2:mRFP in an infected rice cell at 22 hpi showing LTi6B:eGFP apparently outlining vesicles in the BIC. Insets show BIC vesicles at higher magnification. **D.** Two BICs with effector vesicles surrounded by FM4-64-stained plant membranes. Strain KV176 expressing Pwl2:eGFP shown as merged eGFP and FM4-

1053 64 fluorescence. On the left, a side-BIC at 19 hpi shows effector vesicles (eGFP fluorescence alone
1054 in the inset) immersed in FM4-64 staining. On the right, a top-down view of a different BIC at 22
1055 hpi, image focus plane just below the BIC. Arrows indicate Pwl2:eGFP vesicles near the BIC.
1056 Images are projections of confocal optical sections. See Supplemental Movie S2 for yet another
1057 side-BIC. Note that in all three cases, lack of FM4-64 staining of the fungal septa and vacuolar
1058 membrane indicates that the EIHM was intact surrounding each IH. **E.** Quantification of BICs
1059 stained by the endocytosis tracer dyes FM4-64 or FM1-43. Bar charts are based on means of all
1060 data from three biological replicates (data points show the means of the individual reps); error bars
1061 indicate standard deviation; three times 90 infection sites observed per treatment. Bars = 10 µm.
1062

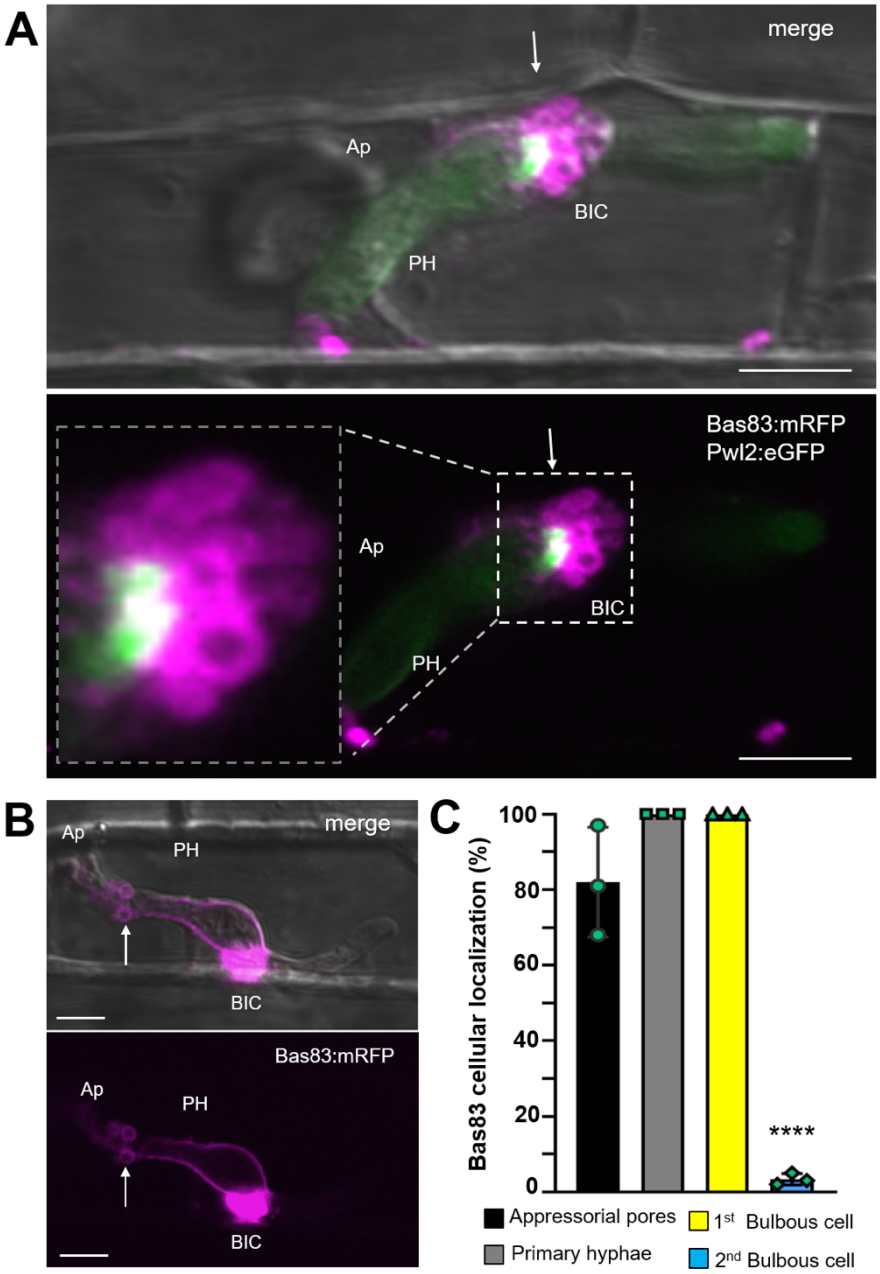

Figure 4. Bas83 is a novel effector associated with membrane vesicles surrounding BICs and BIC-associated cells. A. Bas83:mRFP binds apparent membrane vesicles surrounding a side-BIC (white arrow) labeled with Pwl2:eGFP (strain KV222). **B.** Bas83:mRFP (KV220) binds to bubble-like structures near a primary hypha (white arrow) as well as labeling a BIC and outlining BIC-associated cells. Images (merged bright field, eGFP and mRFP fluorescence) are projections of confocal optical sections. See additional images in Supplemental Figure S4. Bars = 10 µm. **C.** Quantification of the cellular localization of Bas83:mRFP during biotrophic invasion of *M. oryzae* KV220. Bar charts are based on means of all data from three biological replicates (data points show the means of the individual reps); error bars indicate standard deviation. ****P<0.0001; 100 infection sites observed per experiment.

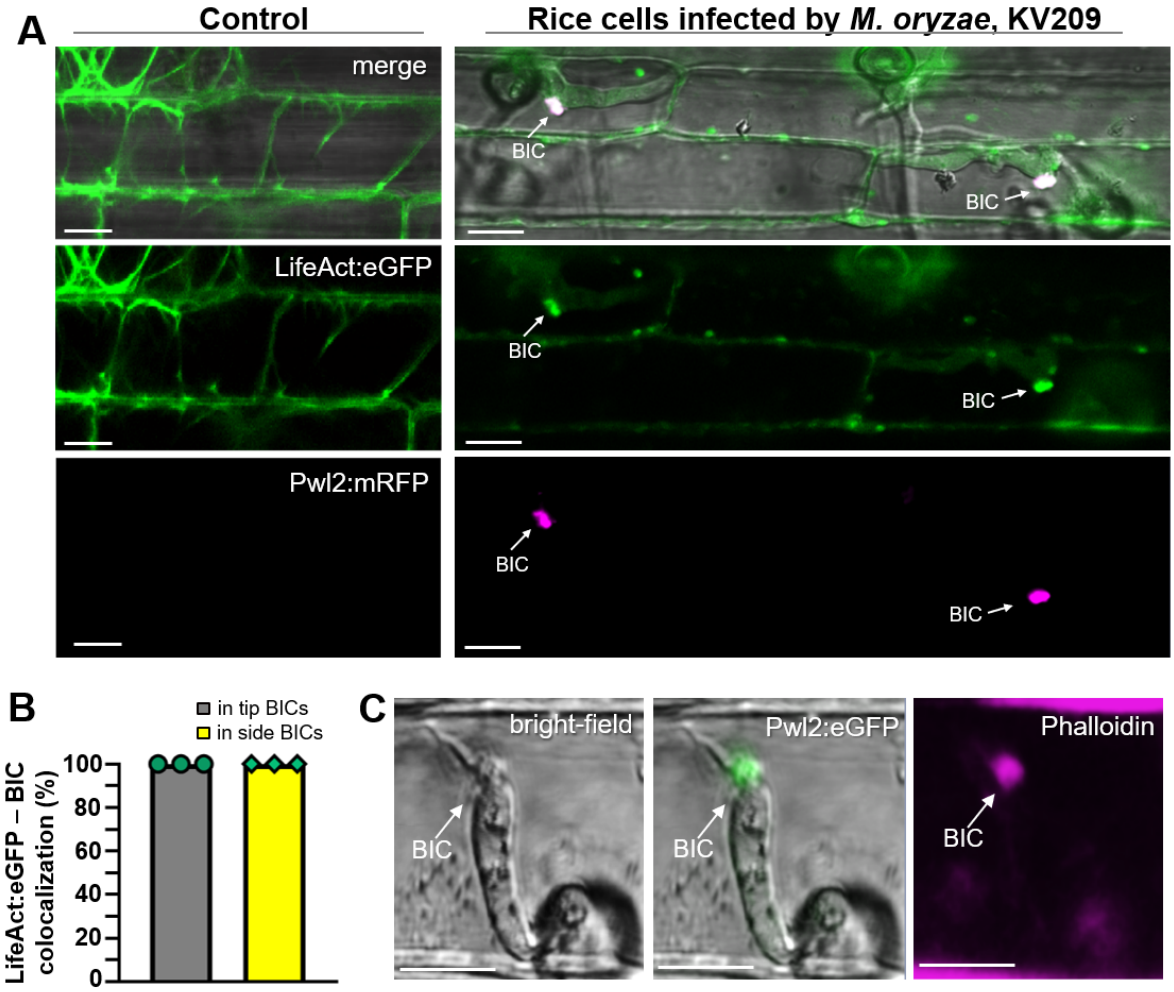

Figure 5. BICs contain plant actin. A. Rice LifeAct:eGFP localization during biotrophic invasion by *M. oryzae*. A rice line expressing LifeAct:eGFP in non-infected cells (left column) and cells infected by *M. oryzae* strain KV209 expressing Pwl2:mRFP in BICs (right column). Colocalization shows BICs are rich in plant actin. **B.** Quantification of the colocalization of LifeAct:eGFP with both tip- and side-BICs. Bar charts are based on means of all data from three biological replicates (data points show the means of the individual reps); error bars indicate standard deviation; three times 100 infection sites observed. **C.** Rhodamine phalloidin conjugate (red fluorescence staining actin, shown as magneta) colocalizes with Pwl2:eGFP (green) in rice cells infected by strain KV176, confirming the actin-rich structure of the BIC.

1086

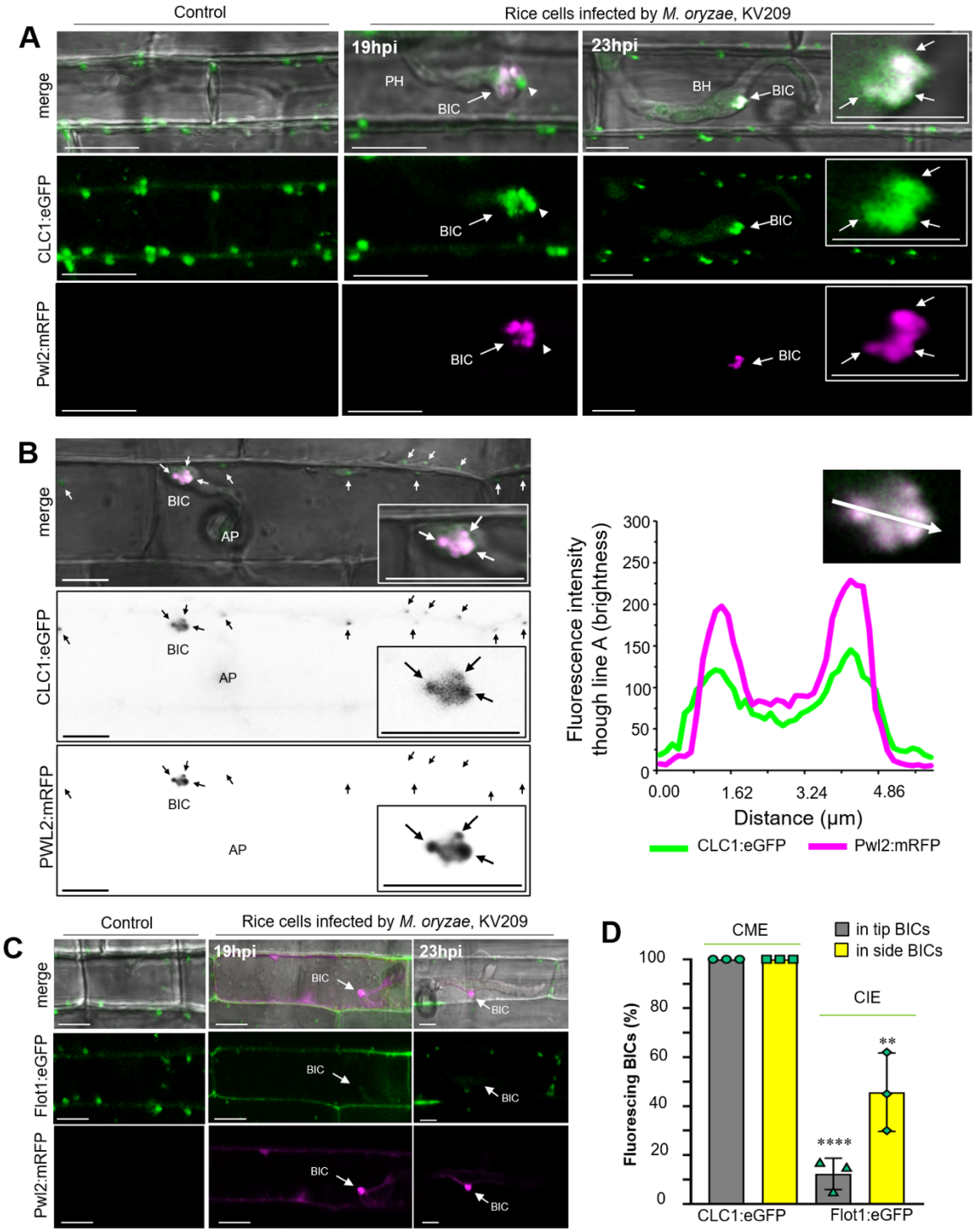

1087

1088 **Figure 6. BICs uniformly contain clathrin, but not in flotillin1. A.** Rice leaf sheaths expressing
1089 CME marker OsCLC1:eGFP were inoculated with strain KV209 expressing Pwl2:mRFP. Shown
1090 from left to right are a non-infected rice sheath cell; an infected cell containing a primary hypha

1091 (PH) with a tip-BIC; and an infected cell containing a bulbous IH (BH) with a side-BIC. Arrows
1092 indicate BICs. Note a vesicle visualized with OsCLC1:eGFP in the tip-BIC (arrowhead) that lacks
1093 Pwl2:mRFP, which is consistent with results in Figure 2A that fluorescent effectors are not always
1094 distributed uniformly in vesicles. (Bars=10µm.) **B.** The fluorescence pattern of OsCLC1:eGFP
1095 (green) corresponds to the Pwl2:mRFP vesicular pattern (magenta), as shown by a fluorescence
1096 intensity linescan along the path of the white arrow. The merge image shows the brightfield view
1097 together with red (magenta) and green fluorescence. Individual black and white inverse images of
1098 CLC1:eGFP and Pwl2:mRFP. Note that this image has been extracted from Supplemental Movie
1099 S3, which shows OsCLC1-labeled effector vesicles in time lapse during tip-BIC to side-BIC
1100 differentiation. **C.** Rice leaf sheaths expressing OsFlot1:eGFP (CIE marker) were inoculated with
1101 KV209 expressing Pwl2:mRFP. From left to right, shown are OsFlot1:eGFP fluorescence in a
1102 non-infected sheath cell; lack of OsFlot1:eGFP fluorescence in a tip-BIC; and lack of
1103 OsFlot1:eGFP fluorescence in a side-BIC. Arrows indicate BICs. Bars=10µm. **D.** Quantification
1104 of the localization of OsCLC1:eGFP or OsFlot1:eGFP at both BIC developmental stages. Bar
1105 charts are based on means of all data from three biological replicates (data points show the means
1106 of the individual reps); error bars indicate standard deviation; three times 97 BICs observed each
1107 treatment. ****$P<0.0001$; **$P=0.002$. CME, clathrin-mediated endocytosis; CIE, clathrin-
1108 independent endocytosis.

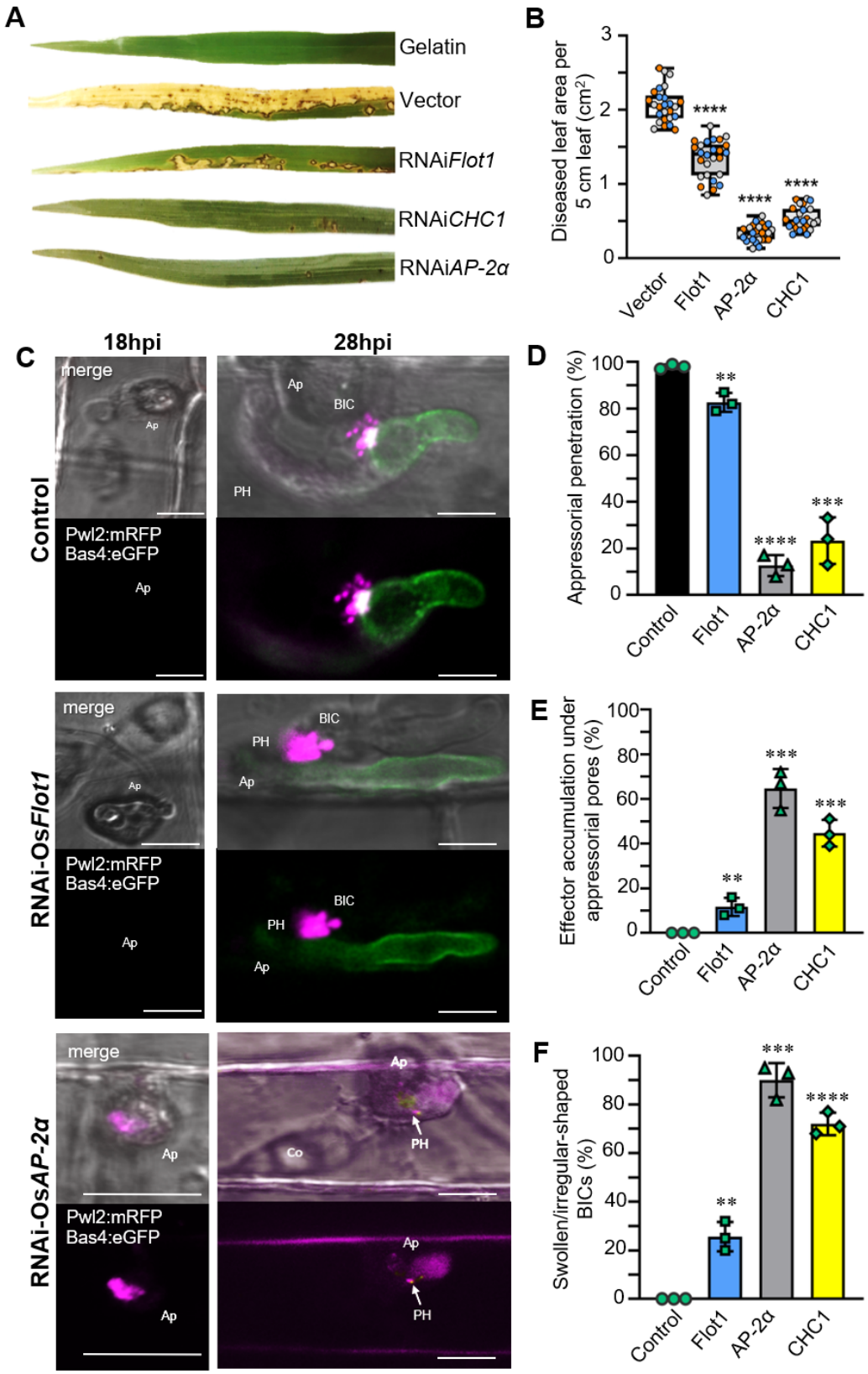
A
Gelatin
Vector
RNAiFlot1
RNAiCHC1
RNAiAP-2α
B
Diseased leaf area per 5 cm leaf (cm2)
Vector
Flot1
AP-2α
CHC1
C
18hpi
28hpi
Control
RNAi-OsFlot1
RNAi-OsAP-2α
merge
Pwl2:mRFP
Bas4:eGFP
Ap
BIC
PH
Co
D
Appressorial penetration (%)
E
Effector accumulation under appressorial pores (%)
F
Swollen/irregular-shaped BICs (%)

1109

1110 **Figure 7. Silencing of rice endocytic machinery suggests roles in pathogenicity and fungal**
1111 **effector translocation. A.** Severity of disease caused by *M. oryzae* strain Guy11 in rice leaves,
1112 cultivar IR64, undergoing silencing of rice endocytic genes**.** Whereas silencing of *Flot1* gene
1113 showed minor effects on pathogenesis, the silencing of the key clathrin-mediated endocytosis
1114 genes, *AP-2*α and CHC1 resulted in a significant reduction in pathogenicity in whole plant spray
1115 inoculation assays. **B.** Quantification of diseased area in 5cm leaf segments in rice expressing
1116 RNAi*AP-2*α, RNAi*CHC1*, RNAi*Flot1* or empty vector infected by strain Guy11. Box and whisker
1117 plots with individual data points are shown; data points of different colors represent different
1118 biological replicates. (P<0.0001 for all treatments; n = 9 rice plants per replication). **C.** Effects of
1119 silencing rice endocytosis genes on the localization of Pwl2:mRFP and Bas4:eGFP during
1120 biotrophic invasion. Wild type IR64 rice and rice expressing RNAi*Flot1* or RNAi*AP-2*α were
1121 infected by KV217 expressing Pwl2:mRFP and Bas4:eGFP at 26 hpi. Note the accumulation of
1122 Pwl2:mRFP under the appressorium (Ap) and the pale Bas4:eGFP fluorescence associated with
1123 the short primary hypha (PH) in the RNAi*AP2*α rice compared to the control and RNAi*Flot1* rice.
1124 Images in C (merged bright field, eGFP and mRFP fluorescence) are shown as projections of
1125 confocal optical sections. Bars = 10 µm. **D.-F.** Quantification of appressorial penetration (D),
1126 effector accumulation under appressoria (E), and swollen irregular BICs (F) in rice expressing
1127 RNAi*Flot1*, RNAi*AP-2*α, RNAi*CHC1* or the empty vector during infection by strain KV209
1128 expressing Pwl2:mRFP (~28 hpi). Bar charts are based on means of all data from three biological
1129 replicates (data points show the means of the individual reps); error bars indicate standard
1130 deviation. (D: **P=0.0031, ***P=0.0002, ****P<0.0001; E: **P=0.0075, ***P=0.0002; F:
1131 **P=0.0018, ****<0.0001; three times 100 infection sites counted per treatment).
1132

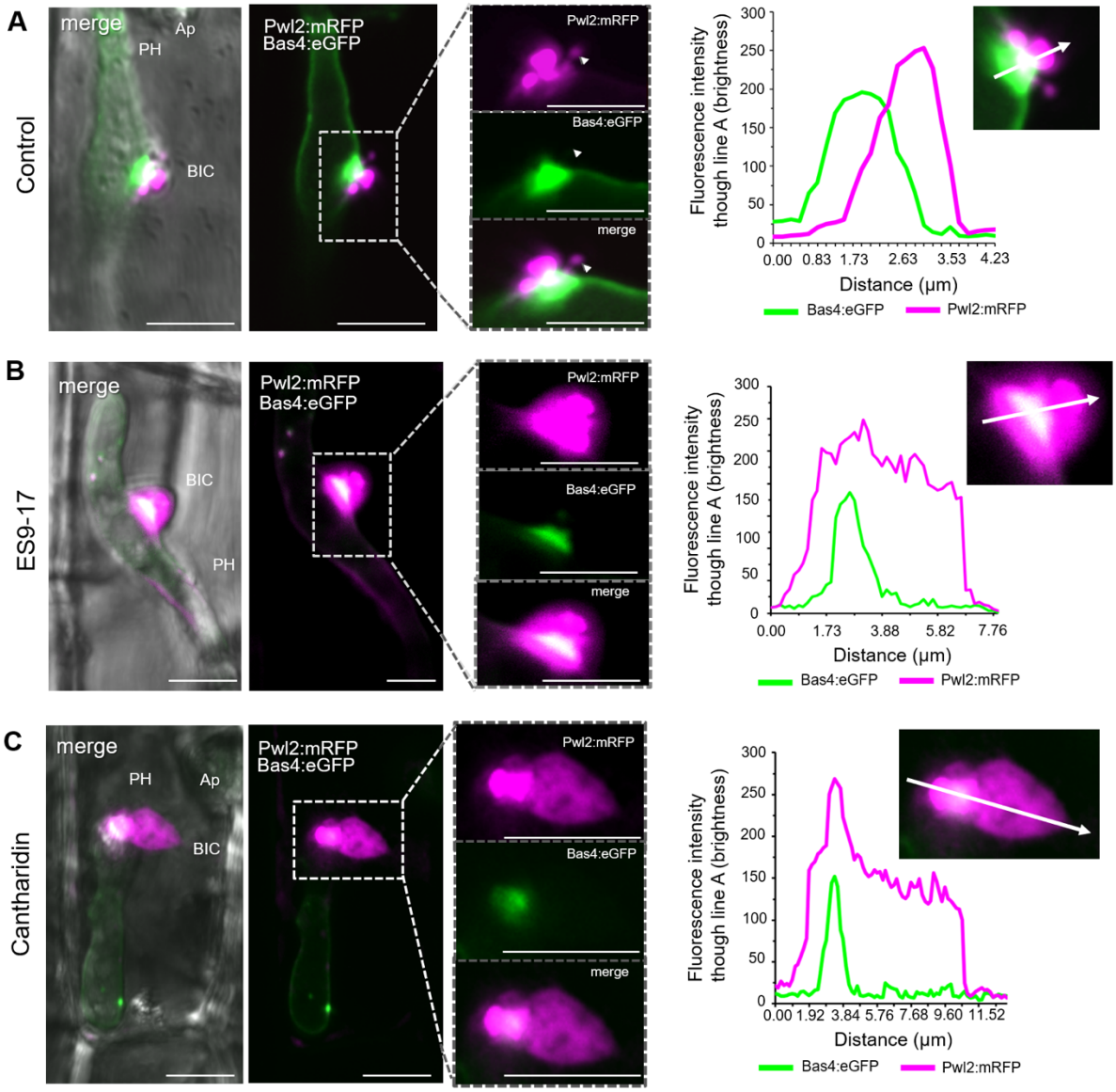

Figure 8. Treatment with CME inhibitor ES9-17 and CME signaling inhibitor cantharidin impacts the localization of cytoplasmic effector Pwl2, but not apoplastic effector Bas4 in BICs. All panels show side-BICs formed during invasion of rice by strain KV217 expressing Pwl2:mRFP and Bas4:eGFP at 26 hpi. **A.** Apoplastic effector Bas4:eGFP identifies an inner base layer of the BIC relative to cytoplasmic Pwl2:mRFP, as shown by fluorescence intensity linescans for GFP (green) and mRFP (magenta) along the path of the white arrow. **B.** After treatment with clathrin heavy chain inhibitor ES9-17, localization of Bas4:eGFP in the BIC base appears unaffected, compared to the non-vesicular swollen localization of Pwl2:mRFP. The white arrows in the inset show the paths for fluorescence intensity distribution linescans for GFP (green) and mRFP (magenta). **C.** After treatment with CME inhibitor cantharidin, localization of Bas4:eGFP in the BIC base appears unaffected, compared to the non-vesicular swollen localization of Pwl2:mRFP, as shown by fluorescence intensity linescans for GFP (green) and mRFP (magenta) along the path of the white arrow. Note linescan distances for Pwl2:mRFP are 2.5 to 3-fold greater

1147 after inhibitor treatments. From left to right, images show merged bright field, eGFP and mRFP
1148 fluorescence; merged eGFP and mRFP fluorescence; insets with enlarged mRFP, eGFP and merge
1149 views; and intensity linescans along the paths of the white arrows. Images are projections of
1150 confocal optical sections. Appressorium (Ap); Primary hypha (PH). Bars = 10 µm.
1151

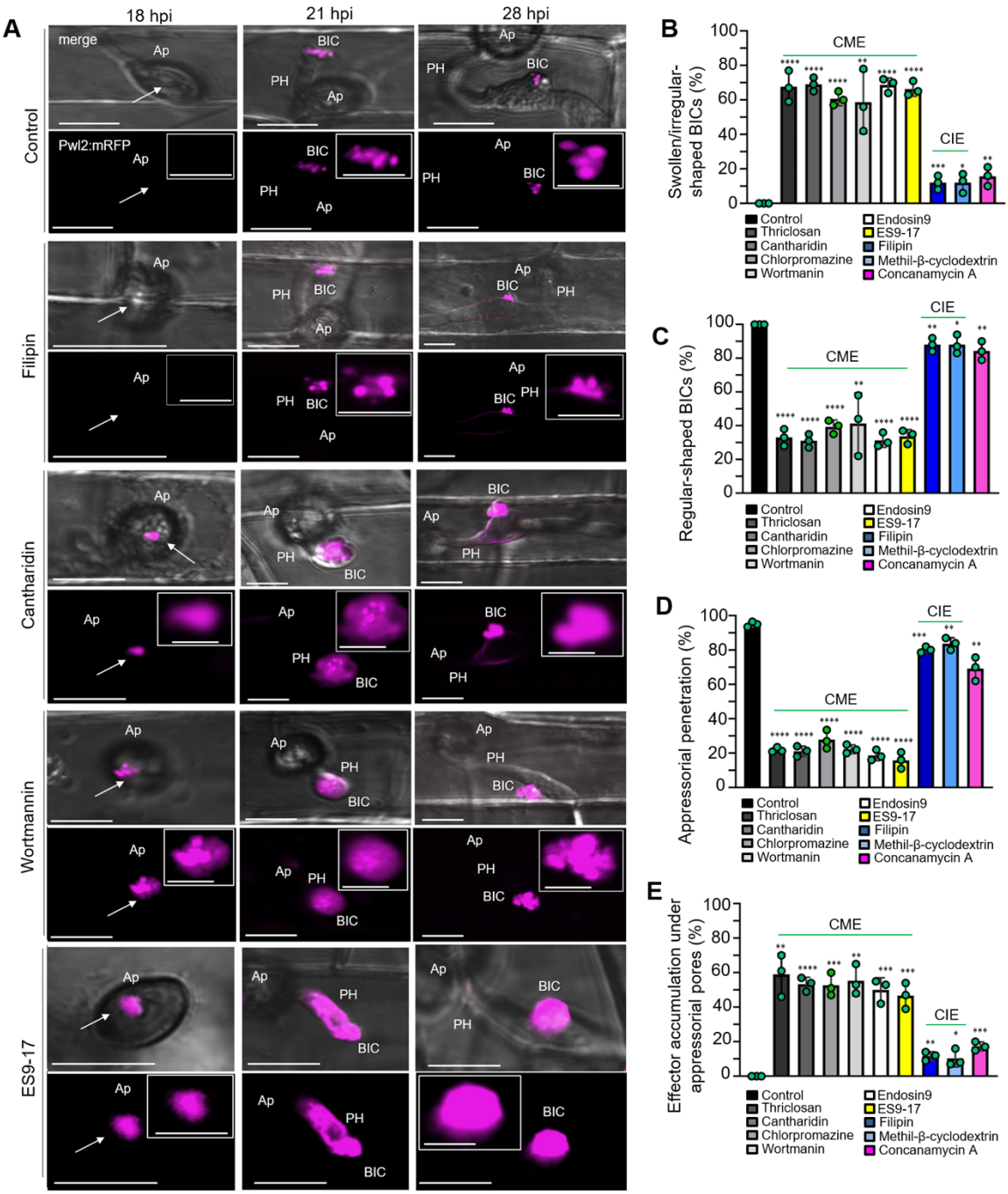

Figure 9. Chemical inhibition of rice CME, but not of CIE, has a major impact on cytoplasmic effector localization in BICs and under appressoria. The chemical inhibitors used are described in Table 1. **A.** Effects of chemical inhibition of clathrin-mediated endocytosis (CME) and clathrin-independent endocytosis (CIE) in the rice sheath assay with strain KV209 expressing Pwl2:mRFP at 18, 21 and 28 hpi. Whereas inhibition of CIE showed minor, although significant, effects on BIC functionality and effector uptake, the chemical inhibition of CME resulted in a significant accumulation of effector fluorescence under appressoria (Ap, white arrows at 18 hpi)

as well as swollen BICs on primary hyphae (PH, 21 hpi) and bulbous IH (28hpi). Images in A (merged bright field and mRFP fluorescence) are projections of confocal optical sections. Insets show close-up views of the effector fluorescence. Bars = 10 µm and bars in the insert boxes = 5 µm. **B-E.** Quantification of swollen, irregular-shaped BICs (B), regular-shaped BICs (C), appressorial penetration (D), and effector accumulation under appressoria (E), in rice undergoing chemical treatment and infection by strain KV209 expressing Pwl2:mRFP at 28 hpi. Bar charts are based on means of all data from three biological replicates (data points show the means of the individual reps); error bars indicate standard deviation. Three times 100 infection sites observed per treatment. B: *P=0.0202(MβC), **P=0.0065(Filipin), **P=0.0079 (Con.A), **P=0.005(Wort.), ****P<0.0001; C: *P=0.02(MβC), **P=0.0065(Filipin), **P=0.0075(Con.A), **P=0.005(Wort.), ****P<0.0001; D: P=0.0068(MβC), **P=0.0004(Filipin), **P=0.0032 (Con.A), ****P<0.0001; E: *P=0.0222(MβC), **P=0.0013(Filipin), ***P=0.0003(Con.A), ***P=0.0002(ES9), ***P=0.0003(ES9-17), **P=0.0004(Wort.), **P=0.0011(Tricl.), ***P=0.0002(Chlorpr.), ****P<0.0001(Canth.).

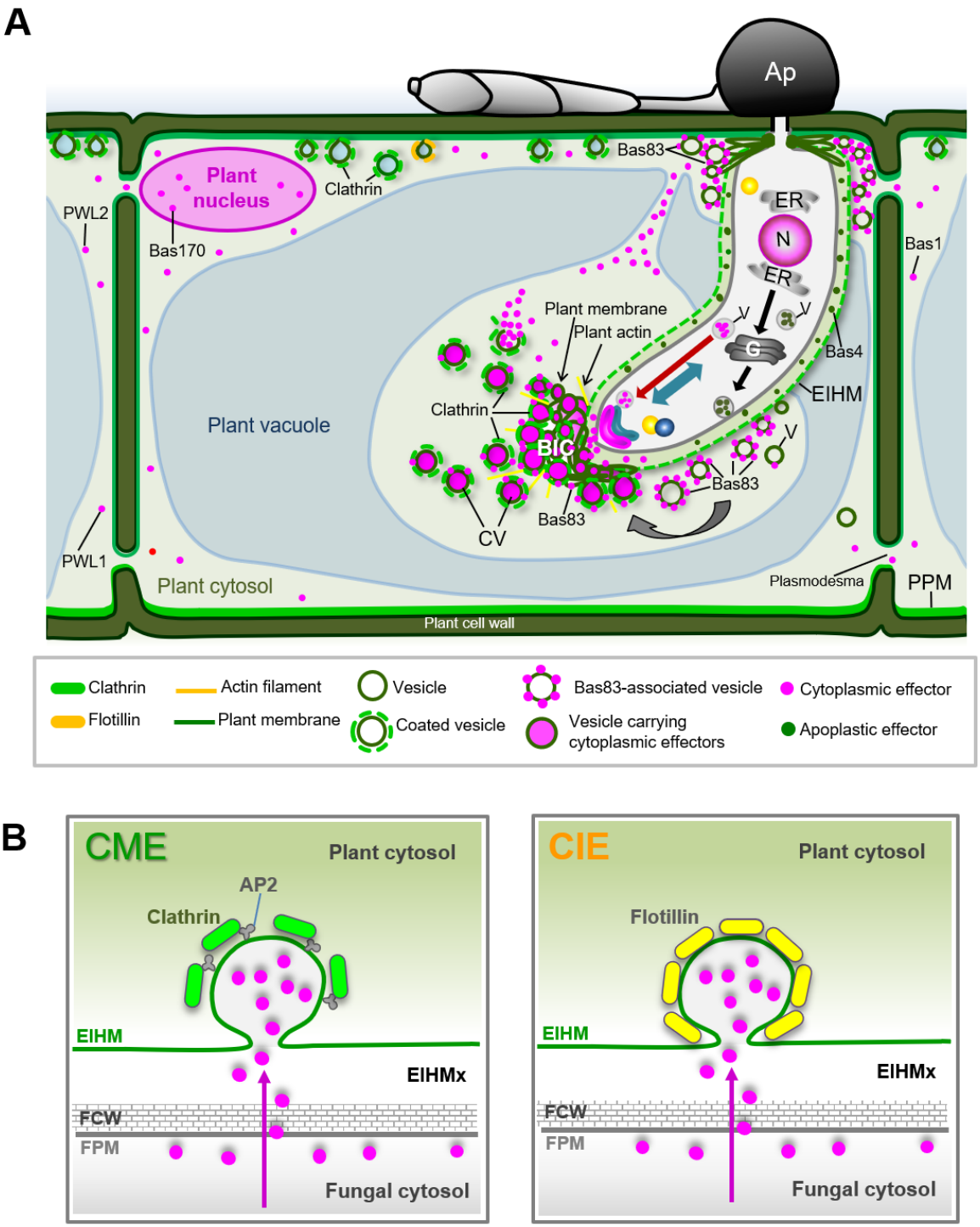

Figure 10. Model for *M. oryzae* effector secretion and translocation into rice cells. A. This cartoon represents the specialized Biotrophic Interfacial Complex at the growing tip of primary hyphae (tip-BIC) at 22–24 h.p.i. (hours post-inoculation), but similar mechanisms apply to side-BICs left behind after differentiation of the first bulbous invasive hyphae (IH). At successful infection sites, apoplastic effectors (dark green circles), including Biotrophy-associated secreted

1180 protein-4 (Bas4), are secreted from the PH by conventional golgi-dependent secretion (black
1181 arrows), which is blocked by treatment with Brefeldin A. Apoplastic effectors accumulate in the
1182 separate compartment enclosed by the EIHM (inside the dark green dashed line around the PH).
1183 In contrast, fluorescently-labeled cytoplasmic effectors (red circles), including Pwl2, Pwl1 and
1184 Bas1, are secreted into BICs by a nonconventional, Brefeldin A-insensitive secretion system
1185 involving the exocyst and SNARE protein Sso1 (red arrows). Cytoplasmic effectors also
1186 accumulate inside the EIHM compartment around the BIC-associated cells, the PH and first
1187 differentiated bulbous IH cell (not shown). In contrast, cytoplasmic effectors do not accumulate in
1188 the EIHM surrounding nonBIC-associated hyphal cells, which are tightly surrounded by the host
1189 vacuole. Our current study expands this model by showing that cytoplasmic effectors are packaged
1190 in dynamic vesicles inside BICs and they can sometimes be observed in the host cytoplasm
1191 surrounding BICs, and that these effector vesicles co-localize with fluorescent plant plasma
1192 membrane markers LTi6B:GFP and FM4-64, as well as clathrin-mediated endocytosis (CME)
1193 marker CLC1:eGFP. These co-localization studies, additional localization with plant actin in BICs,
1194 and functional analyses via VIGS and pharmacological inhibitors support CME as a major
1195 mechanism for effector translocation. Further research should focus on two novel cytoplasmic
1196 effectors we describe. Bas83 labels empty membrane vesicles, possibly recruiting more host
1197 membrane to the BIC and the EIHM surrounding BIC-associated cells. Bas170 localizes to effector
1198 vesicles directly under the appressorium and accumulates in the host nucleus between BICs and
1199 the host cell periphery would facilitate movement of translocated effectors to the host nucleus and
1200 other sites of action in the host cell, as well as movement of cytoplasmic effectors through
1201 plasmodesmata into surrounding host cells to prepare them for invasion. Key: N, fungal nucleus;
1202 ER, endoplasmic reticulum; G, Golgi apparatus; V, transport vesicle. **B.** Working models for
1203 vesicle formation and effector translocation in the rice-*M. oryzae* interaction through CME or
1204 clathrin-independent endocytosis (CIE). Although our current work supports a role for CME, some
1205 involvement of CIE in effector translocation cannot be ruled out as playing a minor role. AP2,
1206 Adaptor Protein-2 complex; EIHM, extrainvasive hyphal membrane; EIHMx, extrainvasive
1207 hyphal matrix; FPM, fungal plasma membrane; FCW, fungal cell wall.